MDEGISPQDLDRRMGSISVAYLGQQQMSEEEIRRIKSMSVPQSKSPFPAKTSKQEKEAVAYLGQKQMS
EEEIQRIKAINLPQVKSPYPAKTNKHAKEALAEAHTWARQPPLCKMYRSQKVMDAHTGADFDLCGLAM
RVYEDVEEKPAAFSGKLILWTFAL**DDYID**GGATFDDPSKTAALLWELSAIIMWSFPDHQYLCQNFANV
VSSGDATQQDAALAWMNRTLADAKRNTGTFYDTSAADCSPFSKALGELWATVAASSPPEFLLRFGISI
QRYVLSNLTEVISRNCKTILPLAEYIEV**R**RRSVAMEVFMVIVEFLNNIYLPDEVFFTPGMQRIITAAN
DIVAWL**NDICSFKKE**ILQGDLCNLVGVISNELNCTFEEAAERAFLMSMTRIADLDKDISDLRRITPPE
HRTGVEMYIQASTNWAWRSYEWYCNSK**RY**NFDV

Figure S1. Amino acid sequence of RlMTPSL3 (accession number UJU85540) from *R. lindenbergiana*. Highly conserved motifs are highlighted in bold.

GC/MS

GC/MS analyses were performed on a 5977A GC/MSD system (Agilent, Santa Clara, CA, USA) with a 7890B GC and a 5977A mass selective detector. The GC was equipped with a HP5-MS fused silica capillary column (30 m, 0.25 mm i. d., 0.50 μm film). Specific GC settings were 1) inlet pressure: 77.1 kPa, He at 23.3 mL min^{-1}, 2) injection volume: 1 μL, 3) temperature program: 5 min at 50 °C increasing at 10 °C min^{-1} to 320 °C, 4) 60 s valve time, and 5) carrier gas: He at 1.2 mL min^{-1}. MS settings were 1) source: 230 °C, 2) transfer line: 250 °C, 3) quadrupole: 150 °C and 4) electron energy: 70 eV. Retention indices (*I*) were determined from retention times in comparison to the retention times of *n*-alkanes (C_7-C_{40}).

NMR spectroscopy

NMR spectra were recorded on a Bruker (Billerica, MA, USA) Avance I (300 MHz), Avance I (400 MHz), Avance I (500 MHz), Avance III HD Prodigy (500 MHz) or an Avance III HD Cryo (700 MHz) NMR spectrometer. Spectra were measured in C_6D_6 and referenced against solvent signals (^{1}H-NMR, residual proton signal: δ = 7.16; ^{13}C-NMR: δ = 128.06).[1]

Incubation experiments with recombinant RlMTPSL3

The heterologous expression of RlMTPSL3 in *Escherichia coli* was performed as reported previously.[2] Test incubations were performed with GPP, FPP, GGPP and GFPP (0.5 mg each) dissolved in substrate buffer (100 μL; 25 mM NH_4HCO_3). After dilution with incubation buffer (0.5 mL; 50 mM Tris/HCl, 10 mM $MgCl_2$, 20% glycerol, pH = 8.2), an RlMTPSL3 elution fraction (0.4 mL) was added. The reaction mixtures were incubated at 30 °C with shaking overnight, followed by extraction with cyclohexane (150 μL). The organic layers were dried with $MgSO_4$ and analyzed by GC/MS.

For a preparative scale incubation, FPP (80 mg) was dissolved in substrate buffer (50 mL), followed by addition of incubation buffer (125 mL). The reaction was started by addition of RlMTPSL3 elution fraction (25 mL) from 8 L of expression culture and incubated at 30 °C with stirring overnight. The reaction mixture was then extracted with Et_2O (3 x 100 mL). The organic layers were dried with $MgSO_4$ and concentrated under reduced pressure. Column chromatography on silica gel with n-pentane yielded compound **1** (0.8 mg) as a colorless oil.

Asterisca-1,6-diene (1). Yield: 0.8 mg (3.9 μmol, 2%), from 80.0 mg (209.2 μmol) FPP trisammonium salt. TLC (n-pentane): R_f = 0.83. GC (HP-5MS): *I* = 1369. IR (diamond ATR): $\tilde{\nu}$ / cm^{-1} = 2955 (s), 2923 (s), 2856 (m), 1659 (w), 1453 (m), 1260 (m), 1093 (m), 1017 (m), 801 (m). HR-MS (APCI): calc. for $[C_{15}H_{25}]^+$ *m*/*z* = 205.1951; found: *m*/*z* = 205.1948. Optical rotation: $[\alpha]_D^{25}$ = +20.6 (*c* 0.03, CH_2Cl_2).

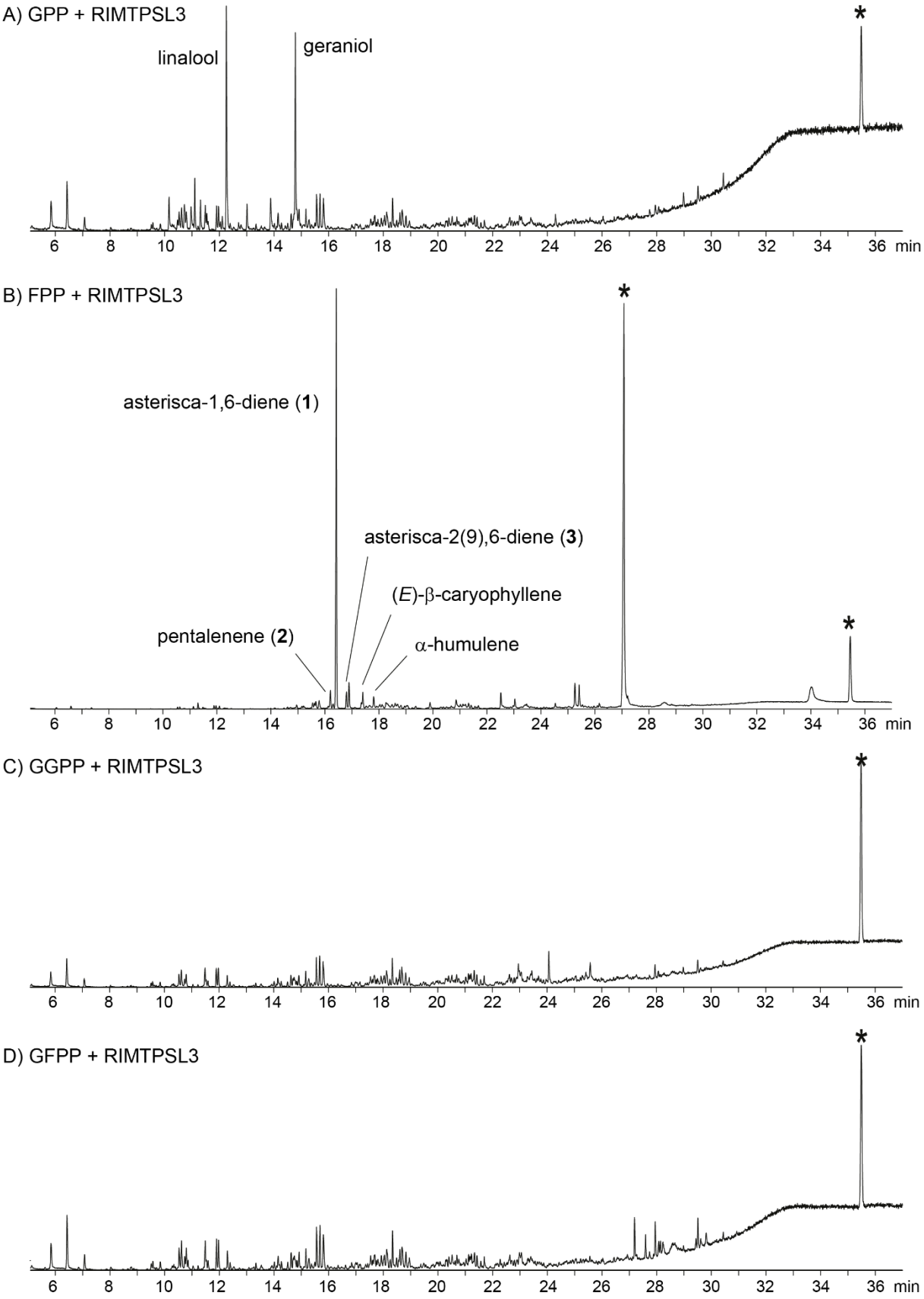

Figure S2. Total ion chromatograms of the products obtained from A) GPP, B) FPP, C) GGPP and D) GFPP. Asterisks indicate contaminants from plasticisers.

Table S1. Identification of terpenes formed by RlMTPSL3.

Compound	*I*[a]	*I* (lit.)[b]	MS match[c]
from GPP:			
linalool	1099	1098[3]	922
geraniol	1254	1254[3]	911
fromFPP:			
pentalenene (**2**)	1355	1339[3]	916
asterisca-1,6-diene (**1**)	1369	–	–
asterisca-2(9),6-diene (**3**)	1397	1381[4]	893
(*E*)-β-caryophyllene	1440	1418[3]	886
α-humulene	1474	1453[3]	914

[a] Retention index on a HP5-MS GC column. [b] Retention index data from the literature on the same or a similar GC column. [c] Mass spectral match factor (0 – 999, 999 indicates identical mass spectra).

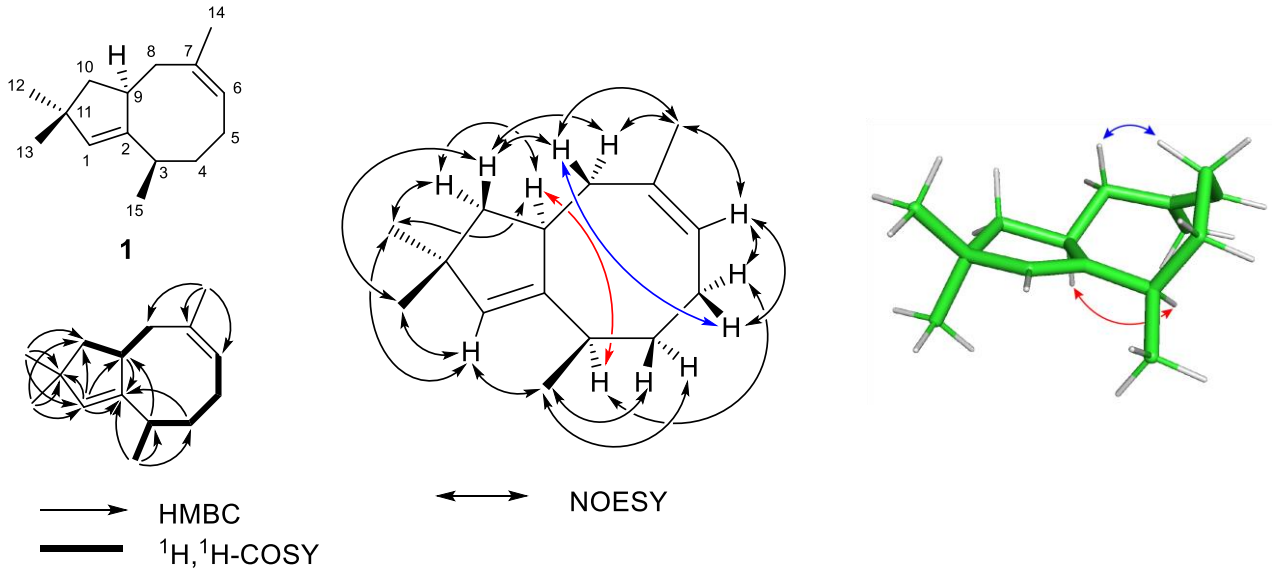

Figure S3. Structure elucidation of **1**. Bold bonds show ^{1}H,^{1}H-COSY correlations, single-headed arrows indicate key HMBC correlations, and double-headed arrows show key NOESY correlations (further HMBC and NOESY correlations are given in Table S2). The stick model in green shows one conformer of **1** that was energy minimized using the MM2 function of Chem3D. This conformer explains the transannular NOESY correlations shown in the ChemDraw structure by the double headed arrows in the same colour.

Table S2. NMR data of asterisca-1,6-diene (**1**) in C_6D_6 recorded at 298 K.

C[a]	type	^{13}C[b]	^{1}H[b]	HMBC[c]	NOESY[d]
1	CH	134.63	5.26 (br s)	2, 3, 9, 10, 11, 12, 13	(4β), 12, 13, 15
2	C_q	151.56	–	–	–
3	CH	31.81	2.09 (m)	1, 2, 4, 9, 15	5α, 9, 15
4	CH_2	38.29	1.52 (dddd, *J* = 12.9, 12.9, 4.9, 4.9, Hα)	2, 3, 5, 6, 15	3, 5α, 15
			1.27 (dddd, *J* = 12.8, 11.9, 5.4, 2.8, Hβ)	2, 3, 5, 6, 15	5α, 5β
5	CH_2	26.37	2.22 (dddd, *J* = 13.1, 13.1, 10.6, 5.3, Hβ)	3, 4, 6, 7	4β, 6, 8β
			1.89 (m, Hα)	3, 4, 6, 7	4α, 4β, 6
6	CH	124.48	5.31 (dd, *J* = 10.5, 6.7)	5, 8, 14	(3), 4α, 5α, 14
7	C_q	136.24	–	–	–
8	CH_2	41.39	2.46 (m, Hβ)	6, 7, 9, 14	5β, 10β, 13
			1.88 (m, Hα)	2, 9, 10, 14	10α, 10β, 14
9	CH	48.33	2.47 (m)	1, 2, 7, 11	12
10	CH_2	47.34	1.97 (dd, *J* = 12.8, 8.4, Hα)	2, 8, 9, 11, 12, 13	9, 12
			1.34 (dd, *J* = 12.8, 2.7, Hβ)	1, 2, 8, 9, 11, 12, 13	8α, 8β, 13
11	C_q	43.66	–	–	–
12	CH_3	30.68	1.08 (s)	1, 10, 11	1, (9), 10α
13	CH_3	31.11	1.13 (s)	1, 10, 11	1, 10β,
14	CH_3	24.90	1.75 (br s)	6, 7, 8	6, 8α, 8β
15	CH_3	22.86	1.07 (d, *J* = 7.0)	2, 3, 4	1, 3, 4α, 4β

[a] Carbon numbering as shown in Figure S3. [b] Chemical shifts δ in ppm, multiplicity: s = singlet, d = doublet, m = multiplet, br = broad, coupling constants *J* are given in Hertz. [c] Numbers of carbons to which HMBC correlations are observed. [d] Hydrogens to which NOESY correlations are observed. Weak correlations are shown in brackets, NOESY correlations to hydrogens at the same carbon are not listed.

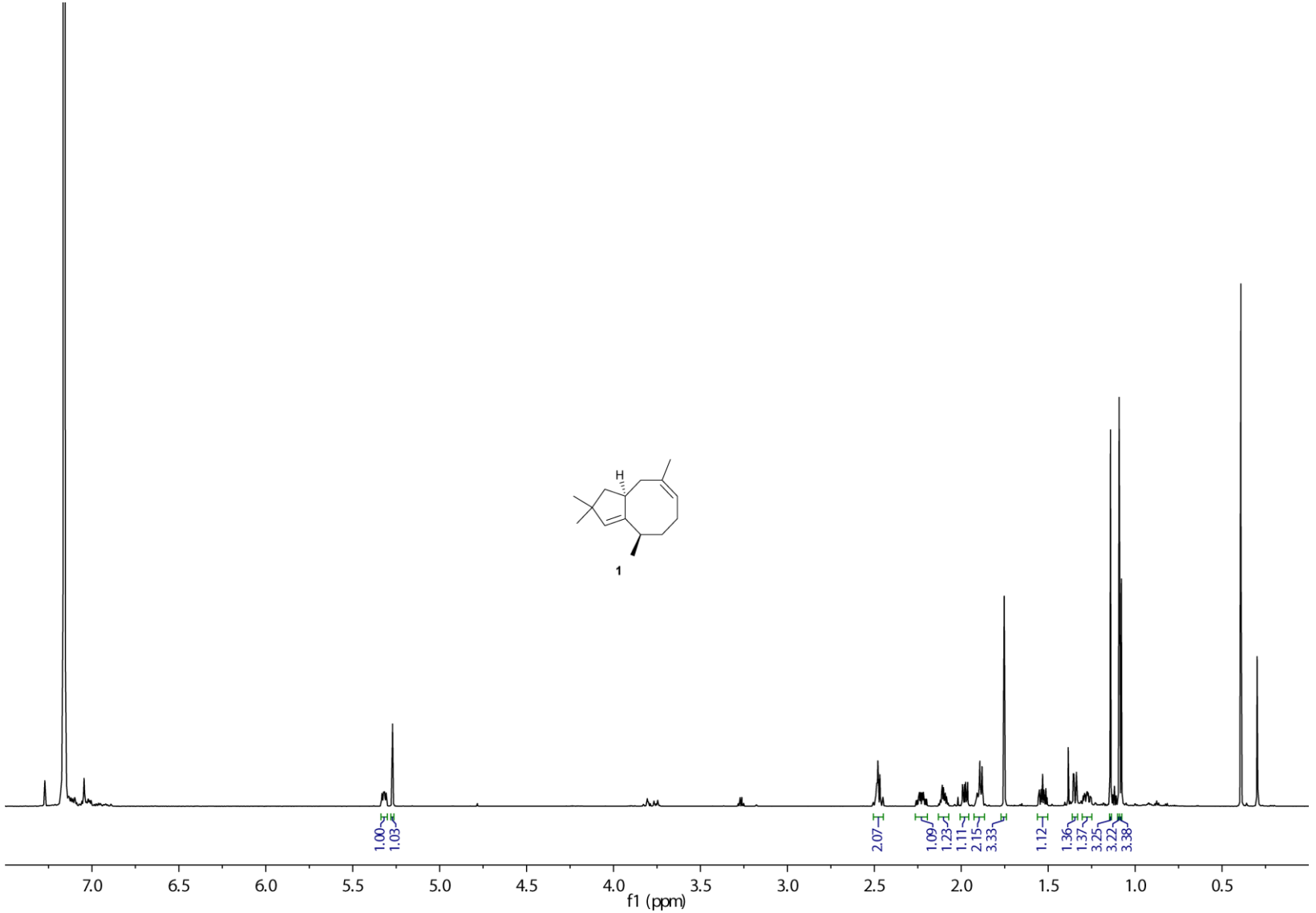

Figure S4. ^{1}H-NMR spectrum of **1** (700 MHz, C_6D_6).

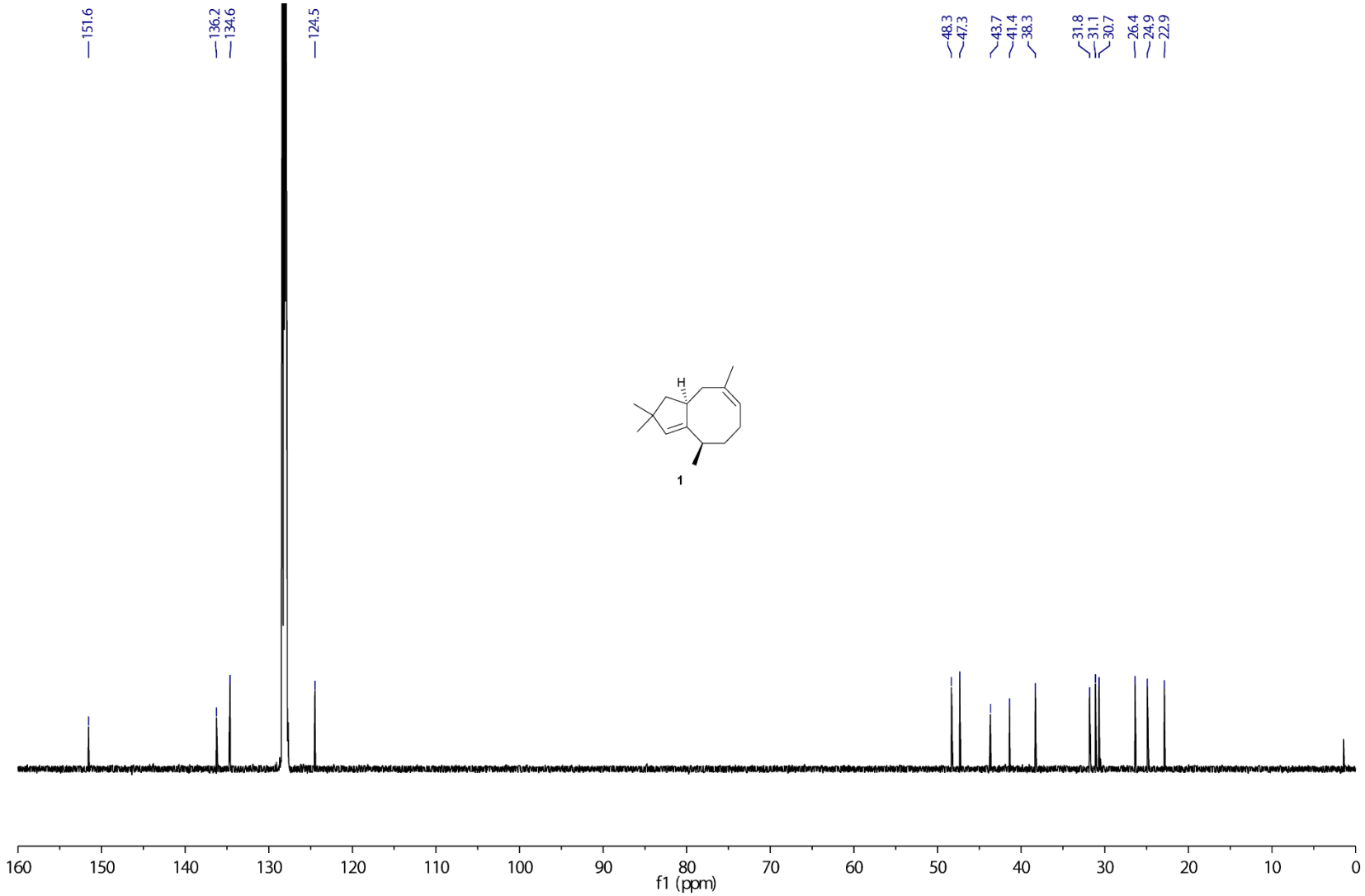

Figure S5. ^{13}C-NMR spectrum of **1** (175 MHz, C_6D_6).

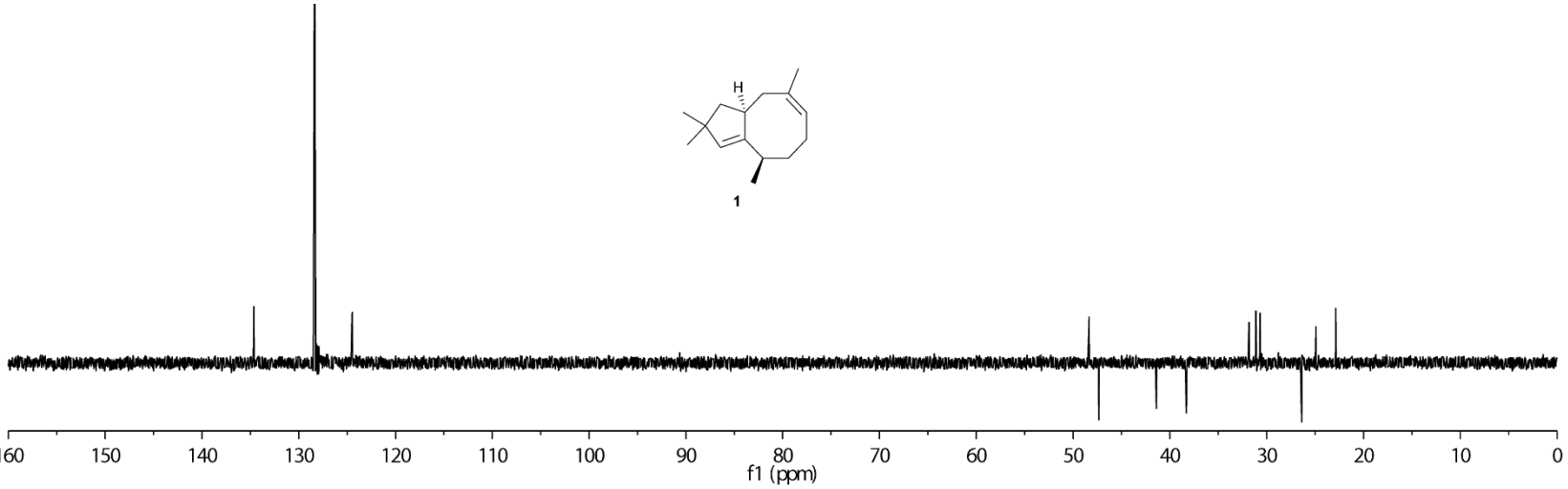

Figure S6. ^{13}C-DEPT-145 spectrum of **1** (175 MHz, C_6D_6).

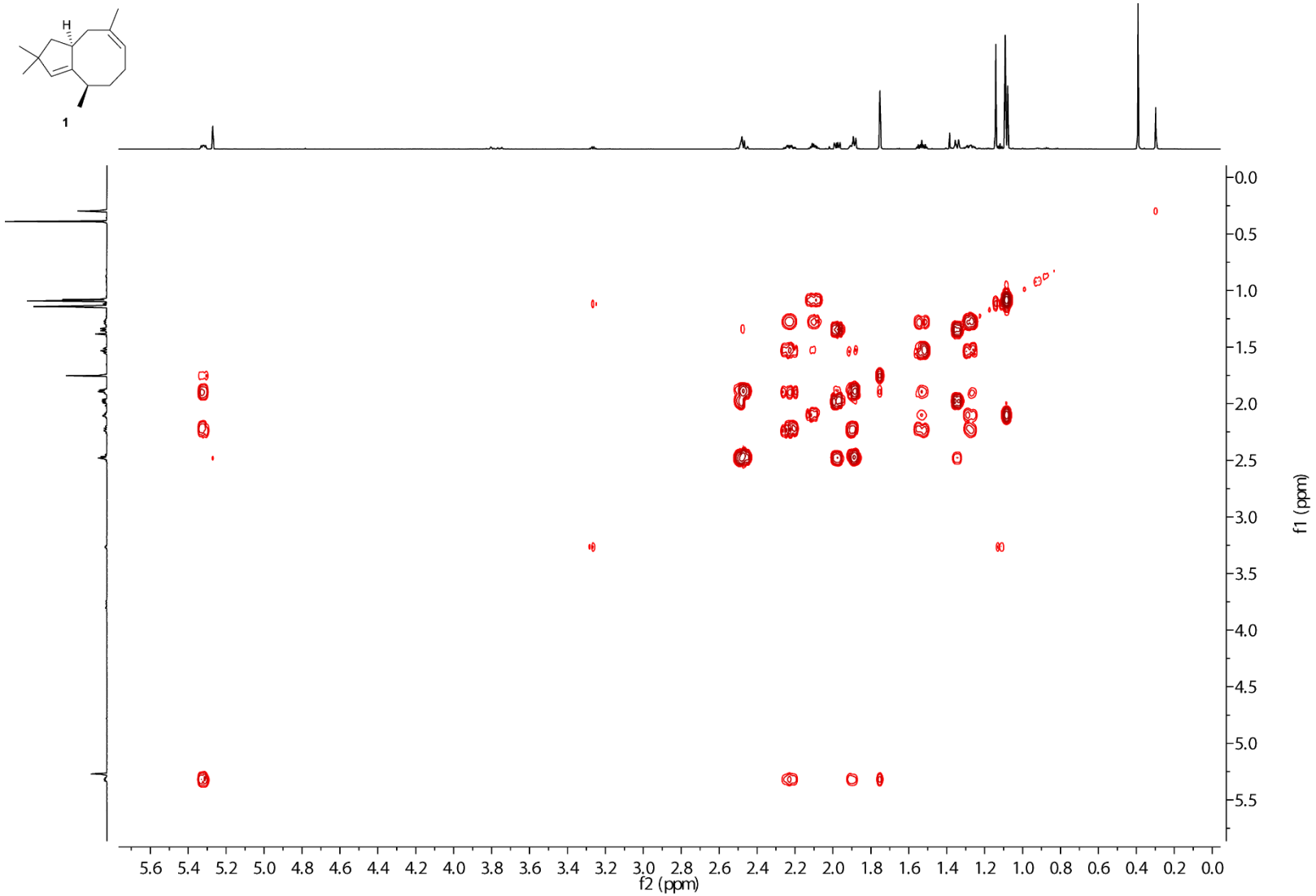

Figure S7. $^{1}H,^{1}H$-COSY spectrum of **1** (C_6D_6).

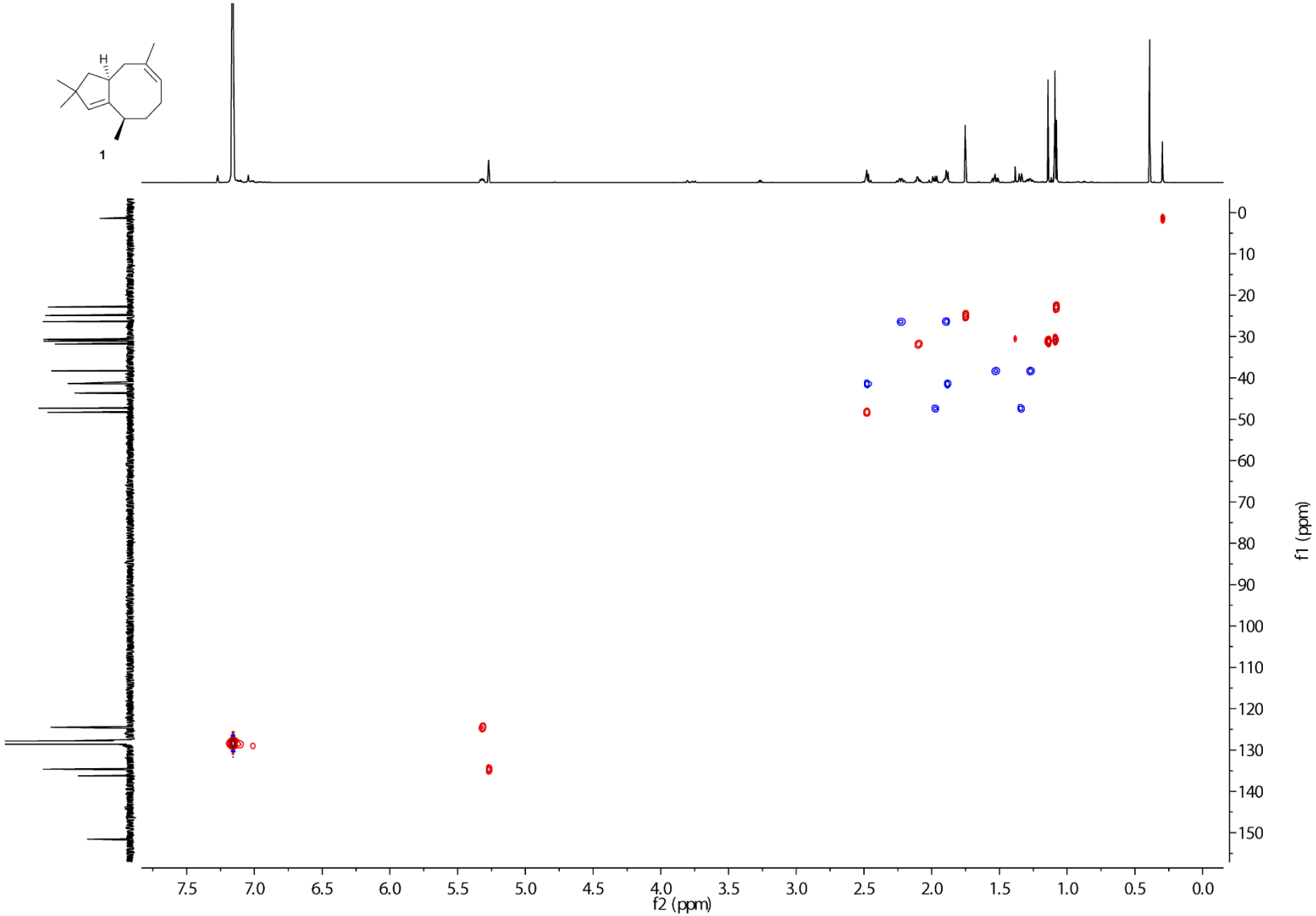

Figure S8. HSQC spectrum of **1** (C_6D_6).

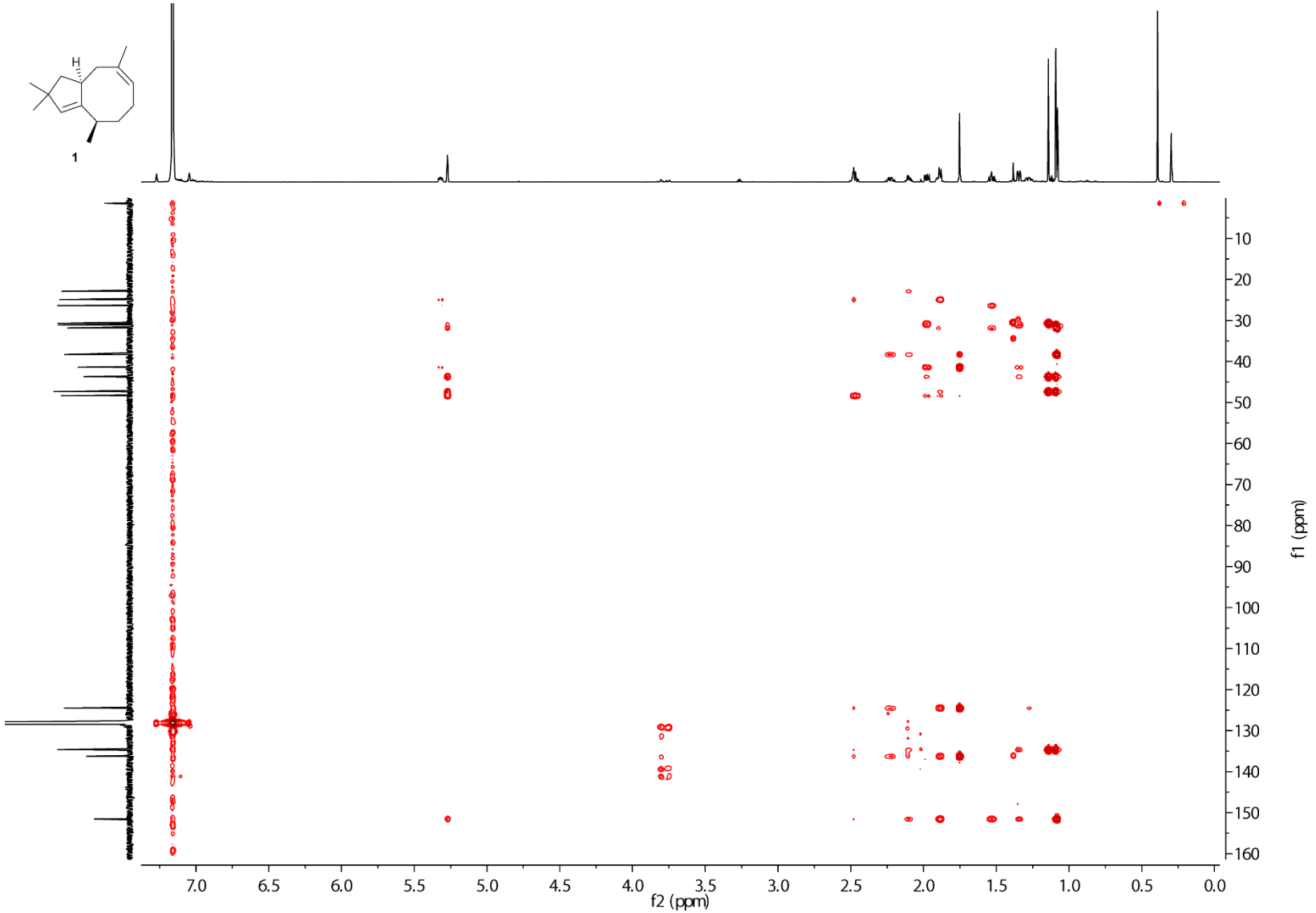

Figure S9. HMBC spectrum of **1** (C_6D_6).

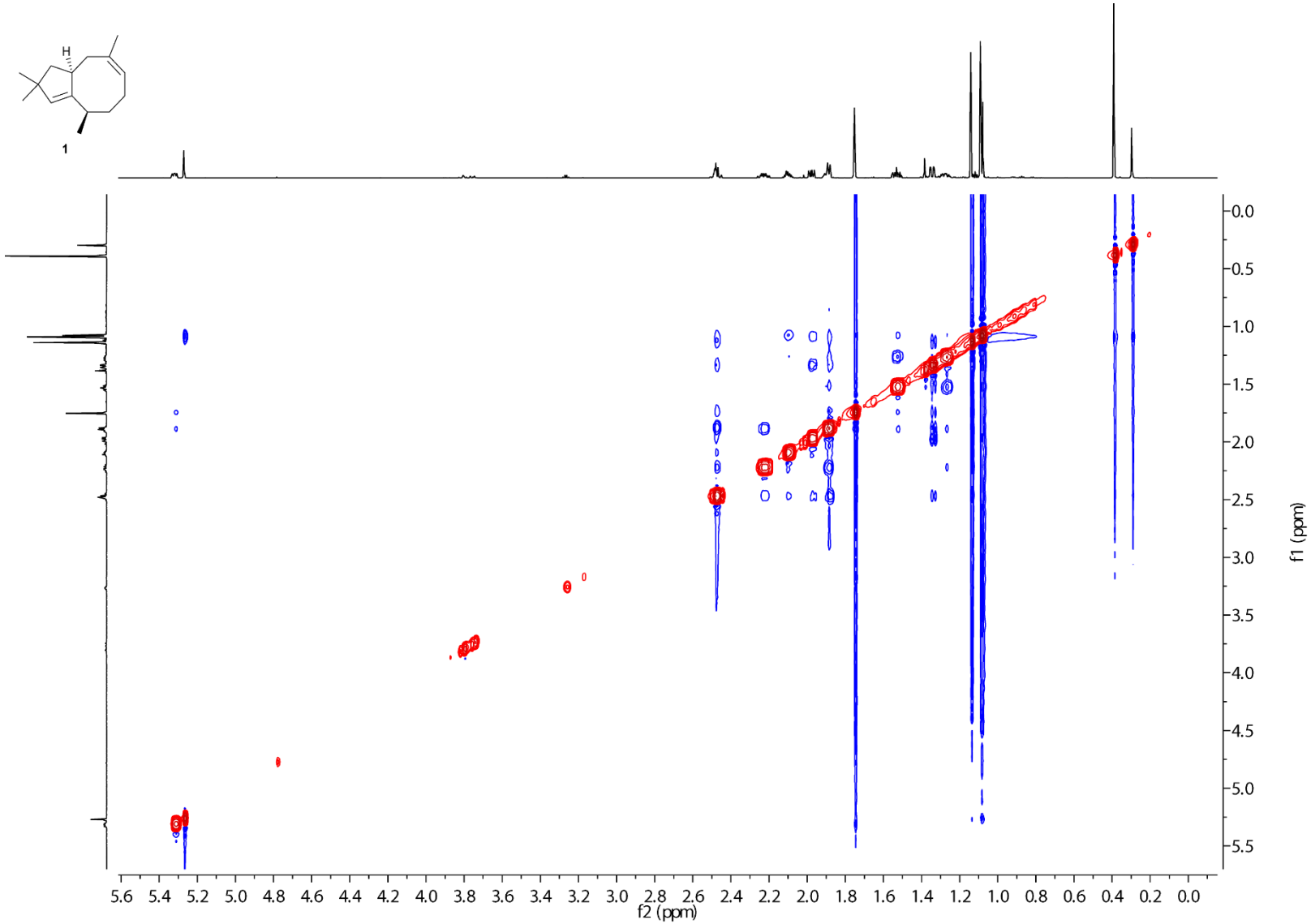

Figure S10. NOESY spectrum of **1** (C_6D_6).

Incubation experiments with isotopically labelled substrates

Isotopic labelling experiments were performed with substrates (ca. 1.0 mg each, in 1 mL 25 mM aq. NH_4HCO_3), incubation buffer (5 mL) and enzyme elution fractions (2 mL each). The substrates and enzyme preparations are listed in Table S3. After incubation at 30 °C with shaking overnight, the products were extracted twice with C_6D_6 (500 μL and 200 μL). The extracts were dried with $MgSO_4$ and analysed by NMR and GC-MS.

Table S3. Labelling experiments with RIMTPSL3.

entry	substrate	enzyme(s)	results shown in
1	DMAPP, (*E*)-(4-^{13}C,4-^{2}H)IPP[5]	FPPS,[6] RIMTPSL3	Figures S11 and S27
2	DMAPP, (*Z*)-(4-^{13}C,4-^{2}H)IPP[5]	FPPS, RIMTPSL3	Figures S11 and S27
3	(*R*)-(1-^{13}C,1-^{2}H)IPP[7]	IDI,[7] FPPS, RIMTPSL3	Figures S12, S21, S22 and S25
4	(*S*)-(1-^{13}C,1-^{2}H)IPP[7]	IDI, FPPS, RIMTPSL3	Figures S12, S21, S22 and S25
5	(12-^{13}C)FPP[8]	RIMTPSL3	Figure S24
6	(9-^{13}C)GPP,[9] IPP	FPPS, RIMTPSL3	Figure S24
7	(2-^{13}C,1,1-$^{2}H_2$)DMAPP,[6] IPP	FPPS, RIMTPSL3	Figure S26
8	(3-^{13}C,2-^{2}H)FPP[10]	RIMTPSL3	Figure S28

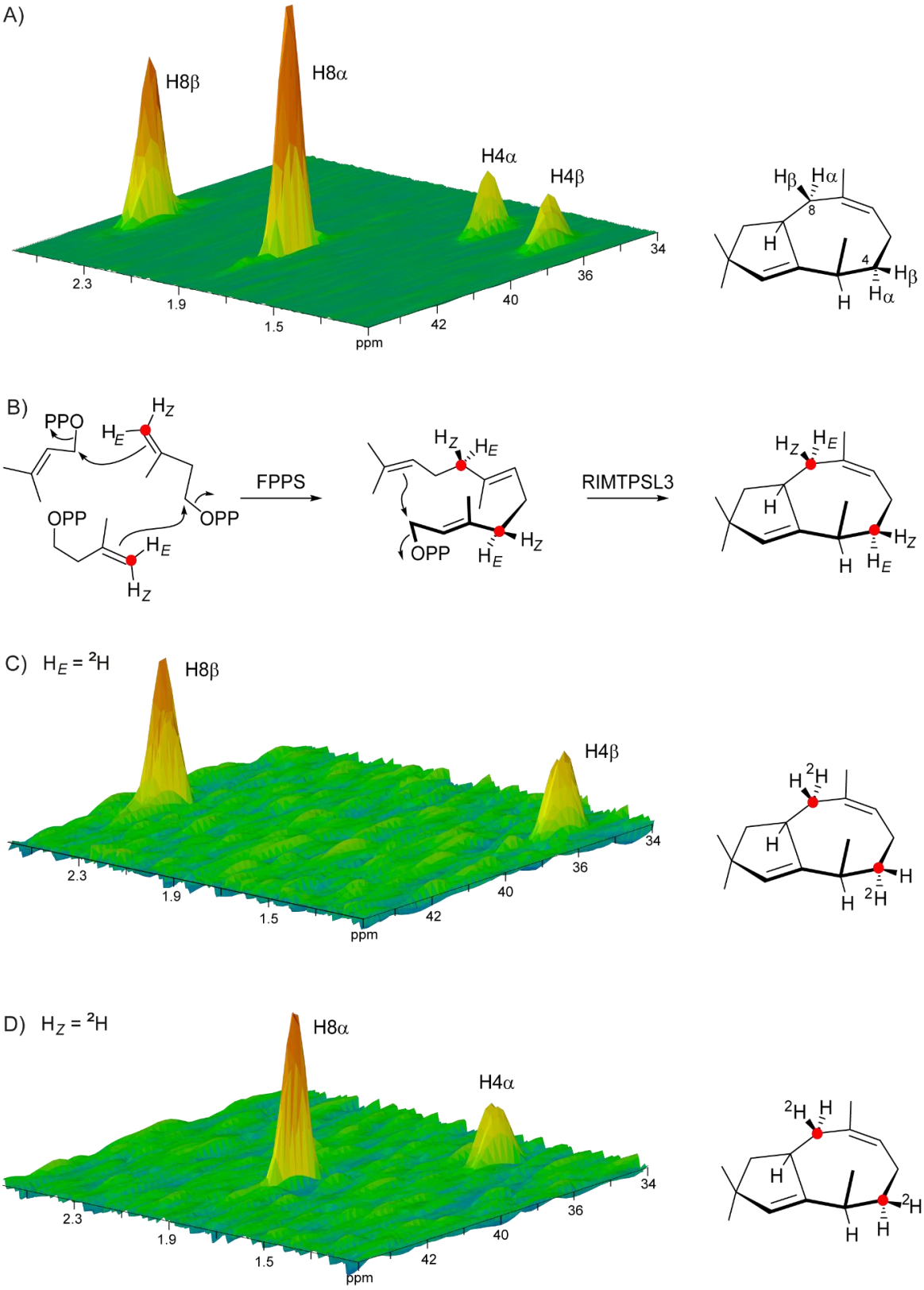

Figure S11. The absolute configuration of **1**. A) Partial HSQC of unlabelled **1** showing the signals for the diastereotopic hydrogens connected to C4 and C8. B) Formation of labelled **1** from DMAPP and (*E*)- or (*Z*)-(4-^{13}C,4-^{2}H)IPP with FPPS and RIMTPSL3. HSQC spectra for C4 and C8 of labelled **1** obtained from C) (*E*)-(4-^{13}C,4-^{2}H)IPP and D) (*Z*)-(4-^{13}C,4-^{2}H)IPP. The artificially introduced stereogenic anchors at C4 and C8 allow to conclude on the absolute configuration of **2** by solving the relative configuration of the naturally present stereogenic centers with respect to these anchors.

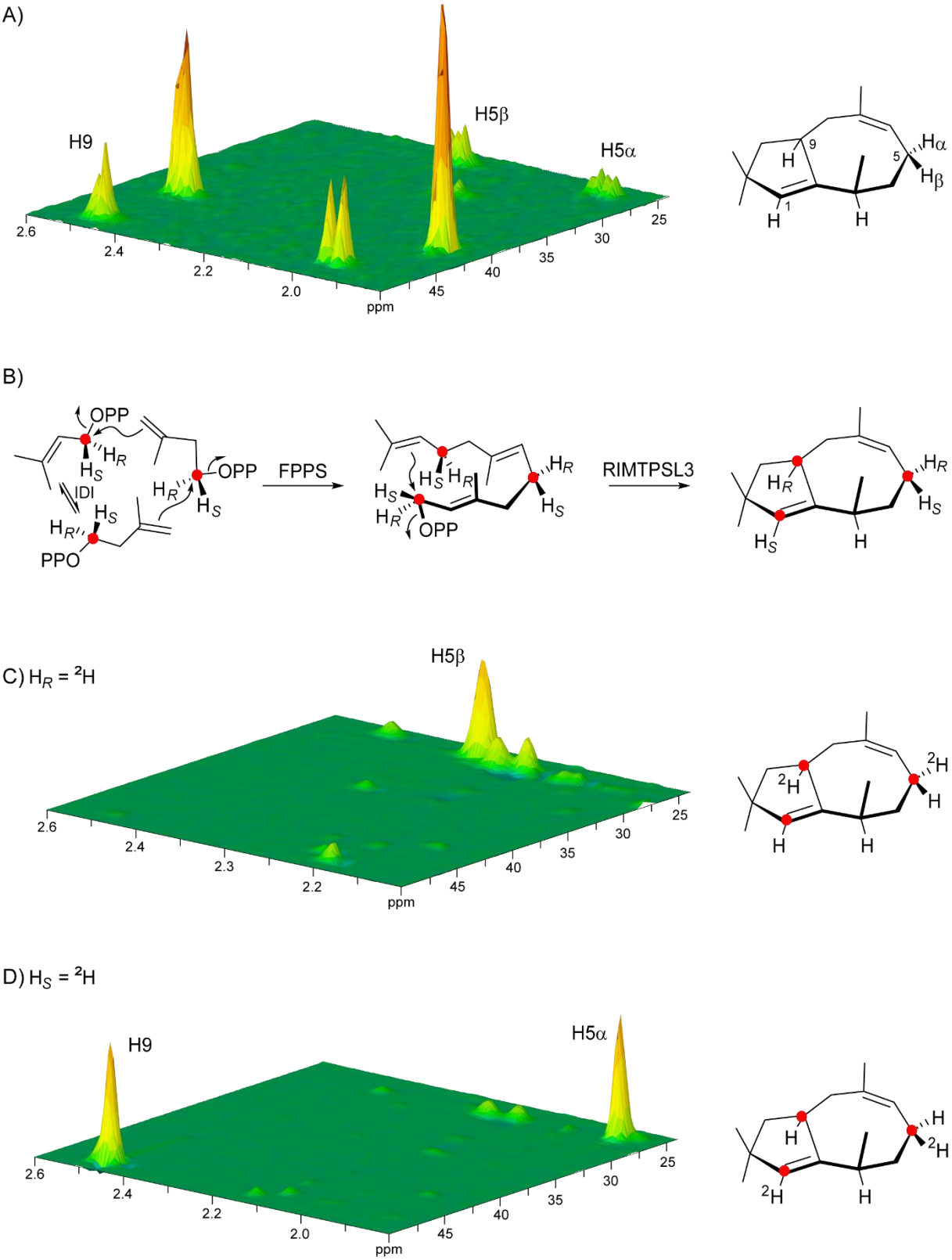

Figure S12. The absolute configuration of **1**. A) Partial HSQC spectrum of unlabelled **1** showing the signals for the diastereotopic hydrogens connected to C5 and the signal for H9. B) Formation of labelled **1** from (*R*)- or (*S*)-(1-^{13}C,1-^{2}H)IPP with IDI, FPPS and RIMTPSL3. HSQC spectra for C5 of labelled **1** obtained from C) (*R*)-(1-^{13}C,1-^{2}H)IPP and D) (*S*)-(1-^{13}C,1-^{2}H)IPP. The artificially introduced stereogenic anchor at C5 allows to conclude on the absolute configuration of **2** by solving the relative configuration of the naturally present stereogenic centers with respect to these anchors. In addition, D) shows a signal for H9 that is not observed in C). In conclusion, H_R is retained at C9.

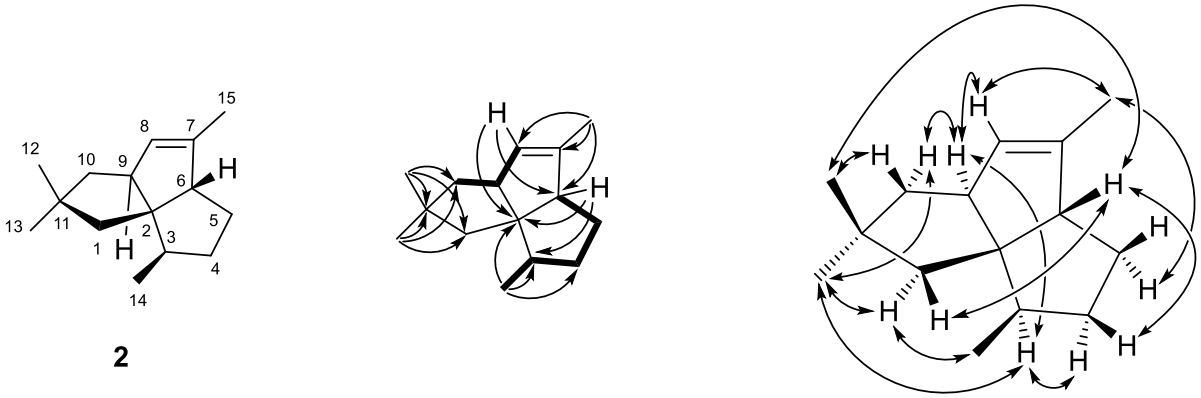

Figure S13. Structure elucidation of **2**.

Table S4. NMR data of pentalenene (**2**) in C_6D_6 recorded at 298 K.

C[a]	type	^{13}C[b]	^{1}H[b]
1	CH_2	49.29	1.74 (d, *J* = 12.9, H_α) 1.37 (d, *J* = 12.9, H_β)
2	C_q	65.10	–
3	CH	45.04	1.82 (m)
4	CH_2	33.84	1.67 (m,H_β) 1.28 (m, H_α)
5	CH_2	27.96	1.77 (m, H_β) 1.35 (m, H_α)
6	CH	62.42	2.52 (m)
7	C_q	140.71	–
8	CH	130.10	5.21 (m)
9	CH	59.90	2.68 (m)
10	CH_2	47.10	1.63 (ddd, *J* = 12.5, 9.2, 1.0, H_α) 1.29 (m, H_β)
11	C_q	40.72	–
12	CH_3	29.33	1.06 (s)
13	CH_3	30.21	1.01 (s)
14	CH_3	17.23	0.90 (d, *J* = 7.1)
15	CH_3	15.62	1.58 (m)

[a] Carbon numbering as shown in Figure S13. [b] Chemical shifts δ in ppm, multiplicity: s = singlet, d = doublet, m = multiplet, coupling constants *J* are given in Hertz.

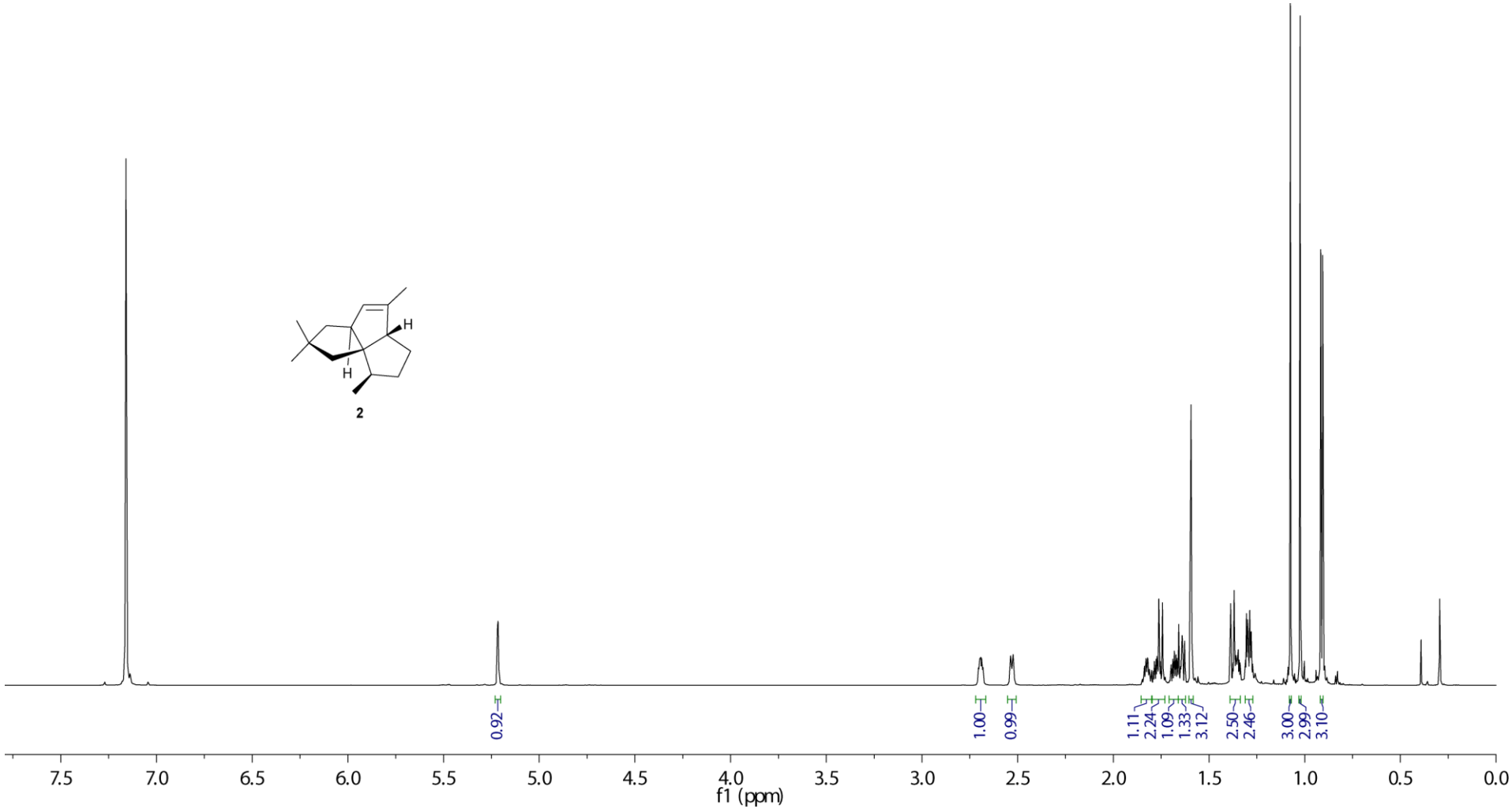

Figure S14. ^{1}H-NMR spectrum of **2** (700 MHz, C_6D_6).

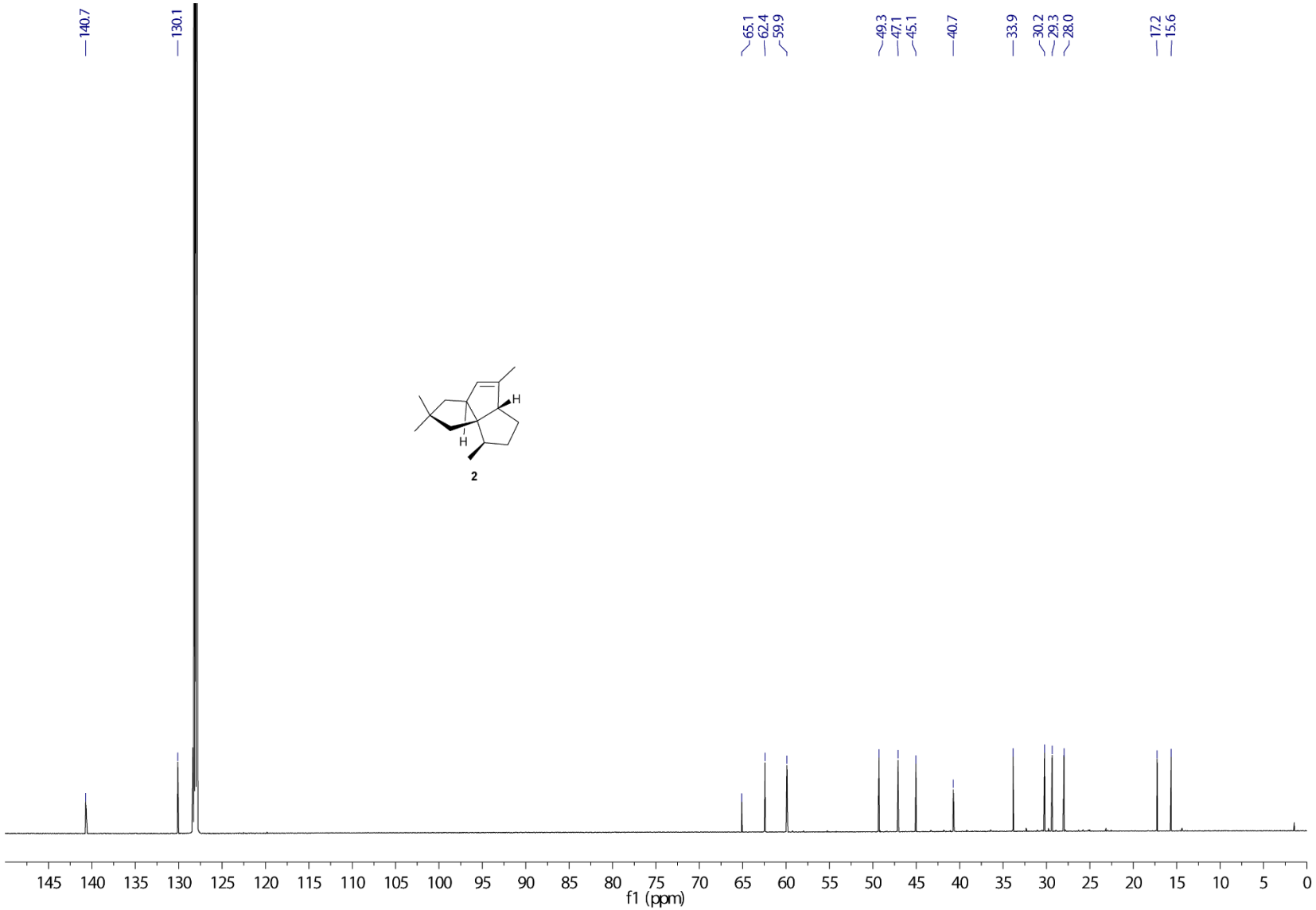

Figure S15. ^{13}C-NMR spectrum of **2** (175 MHz, C_6D_6).

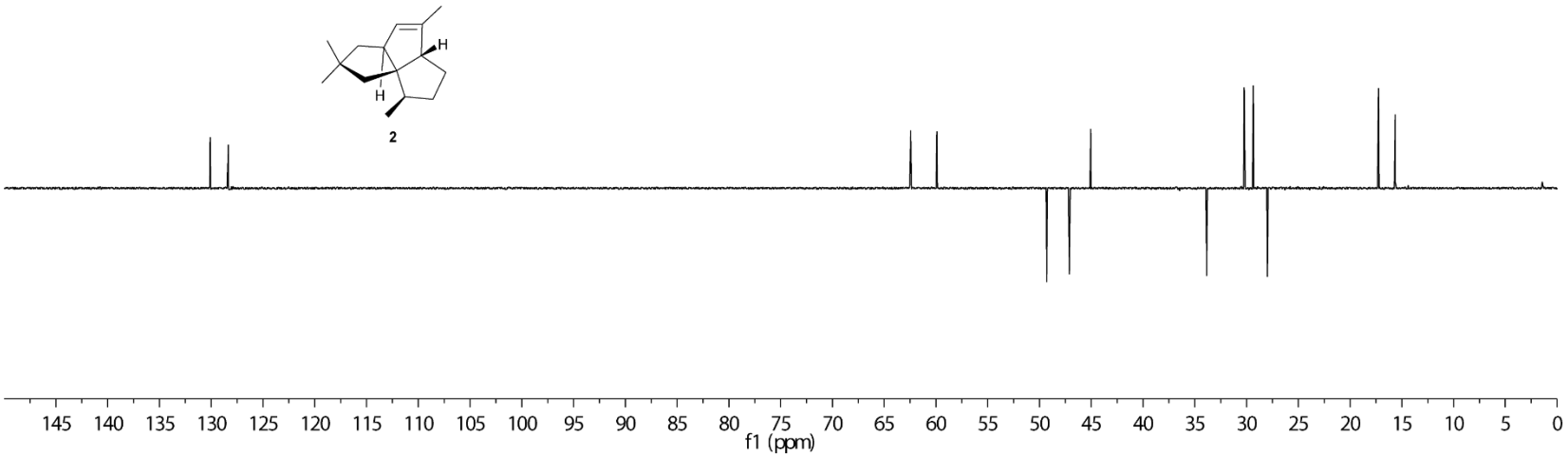

Figure S16. ^{13}C-DEPT-145 spectrum of **2** (175 MHz, C_6D_6).

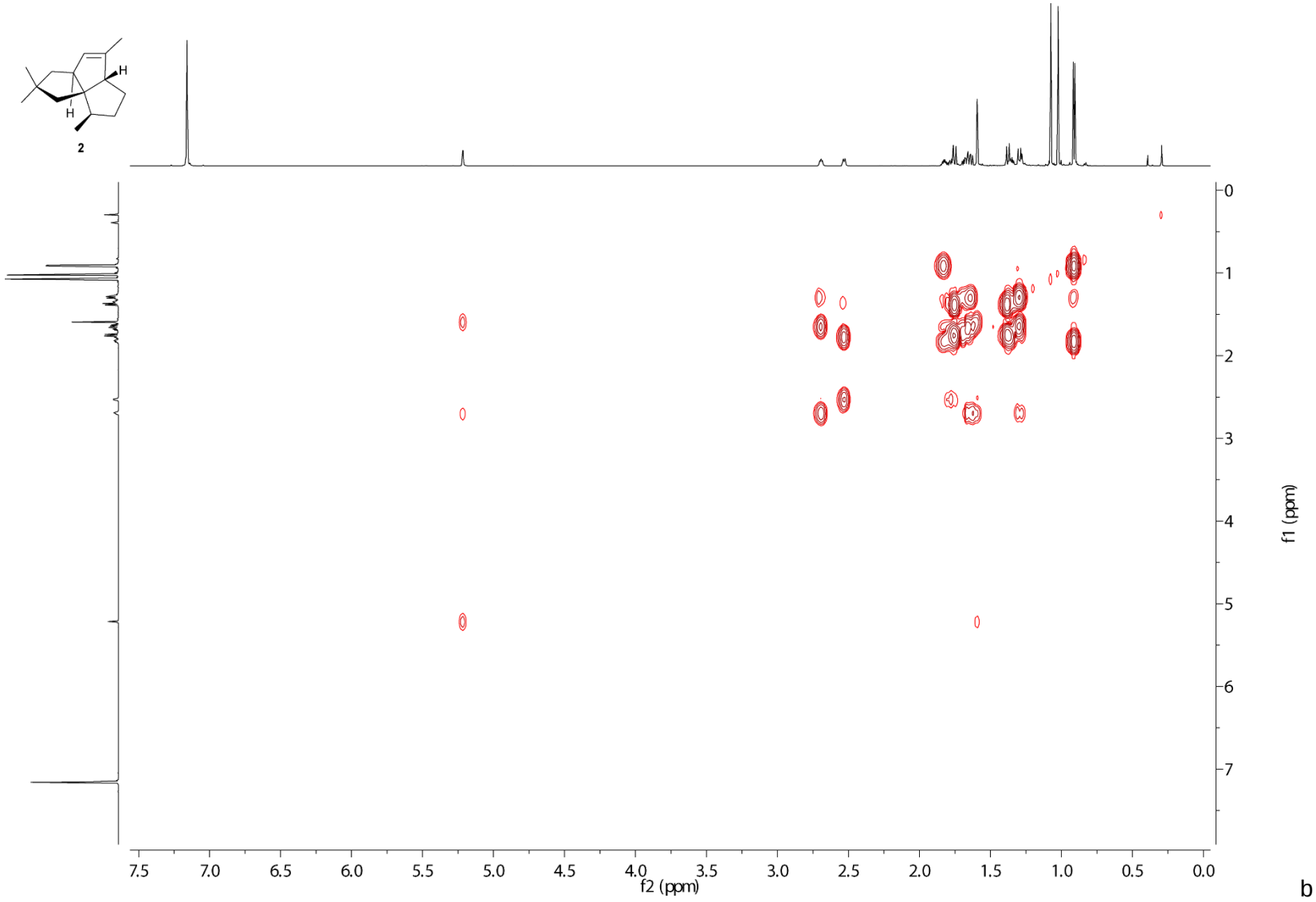

Figure S17. $^{1}H,^{1}H$-COSY spectrum of **2** (C_6D_6).

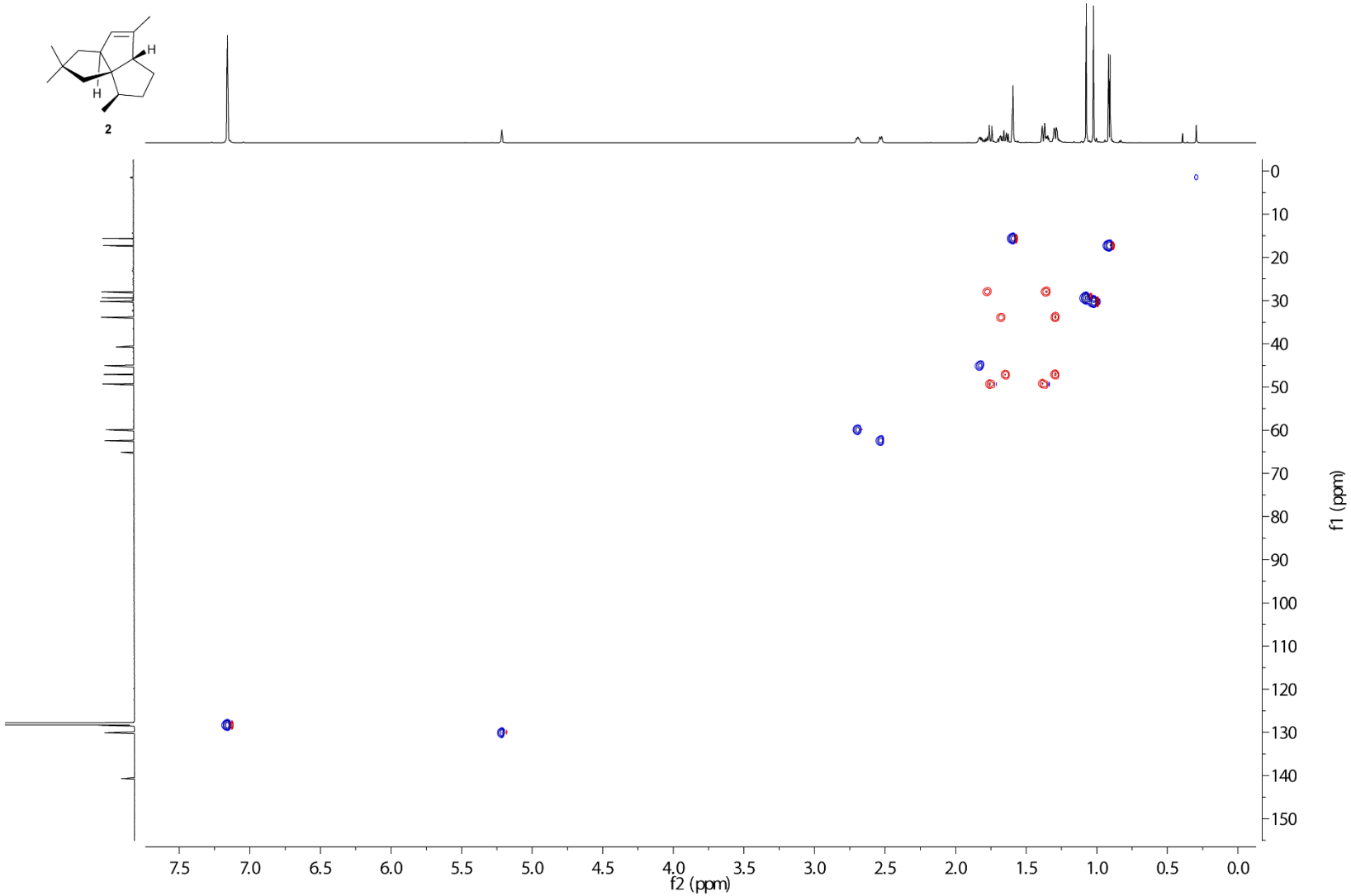

Figure S18. HSQC spectrum of **2** (C_6D_6).

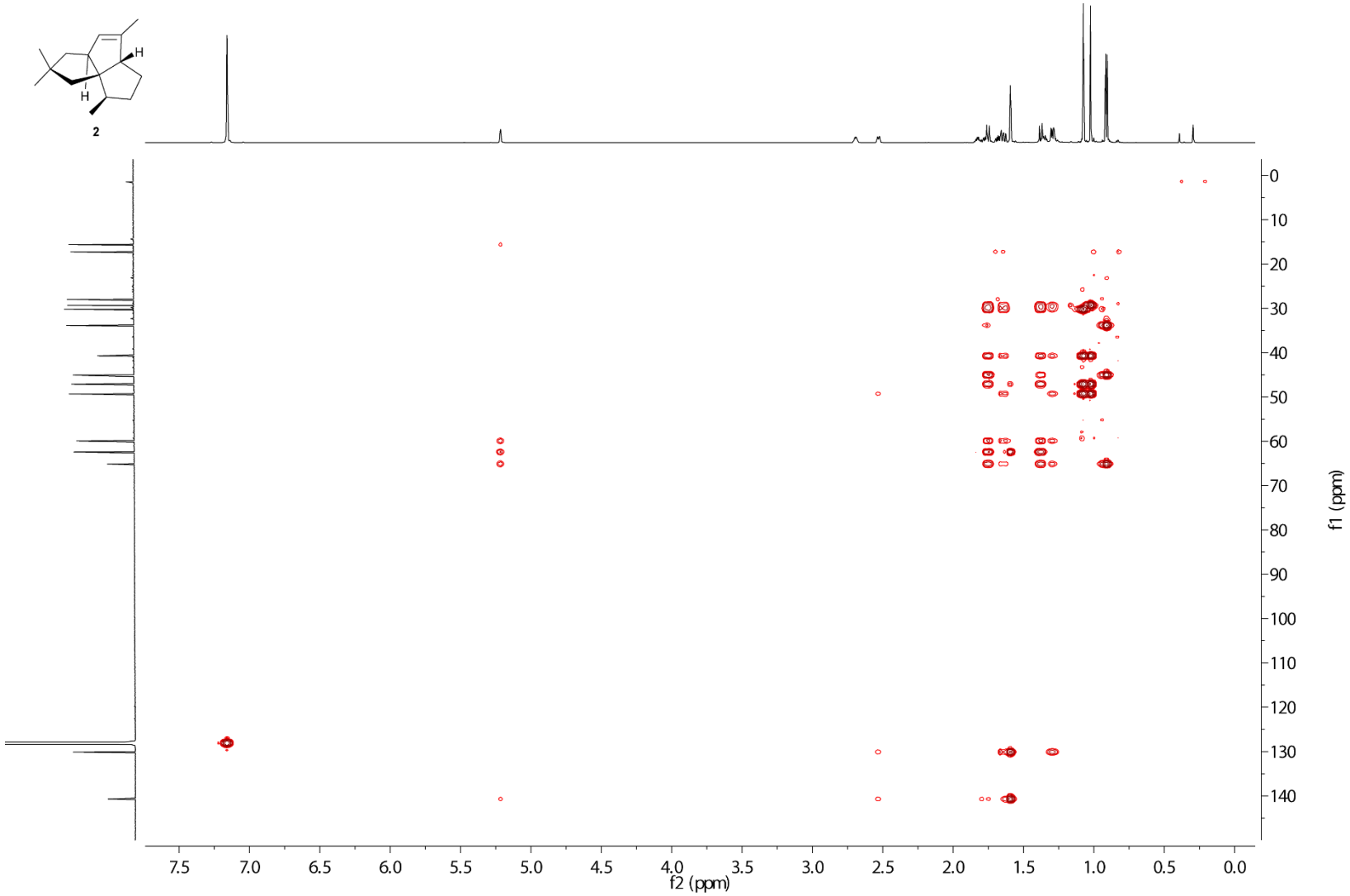

Figure S19. HMBC spectrum of **2** (C_6D_6).

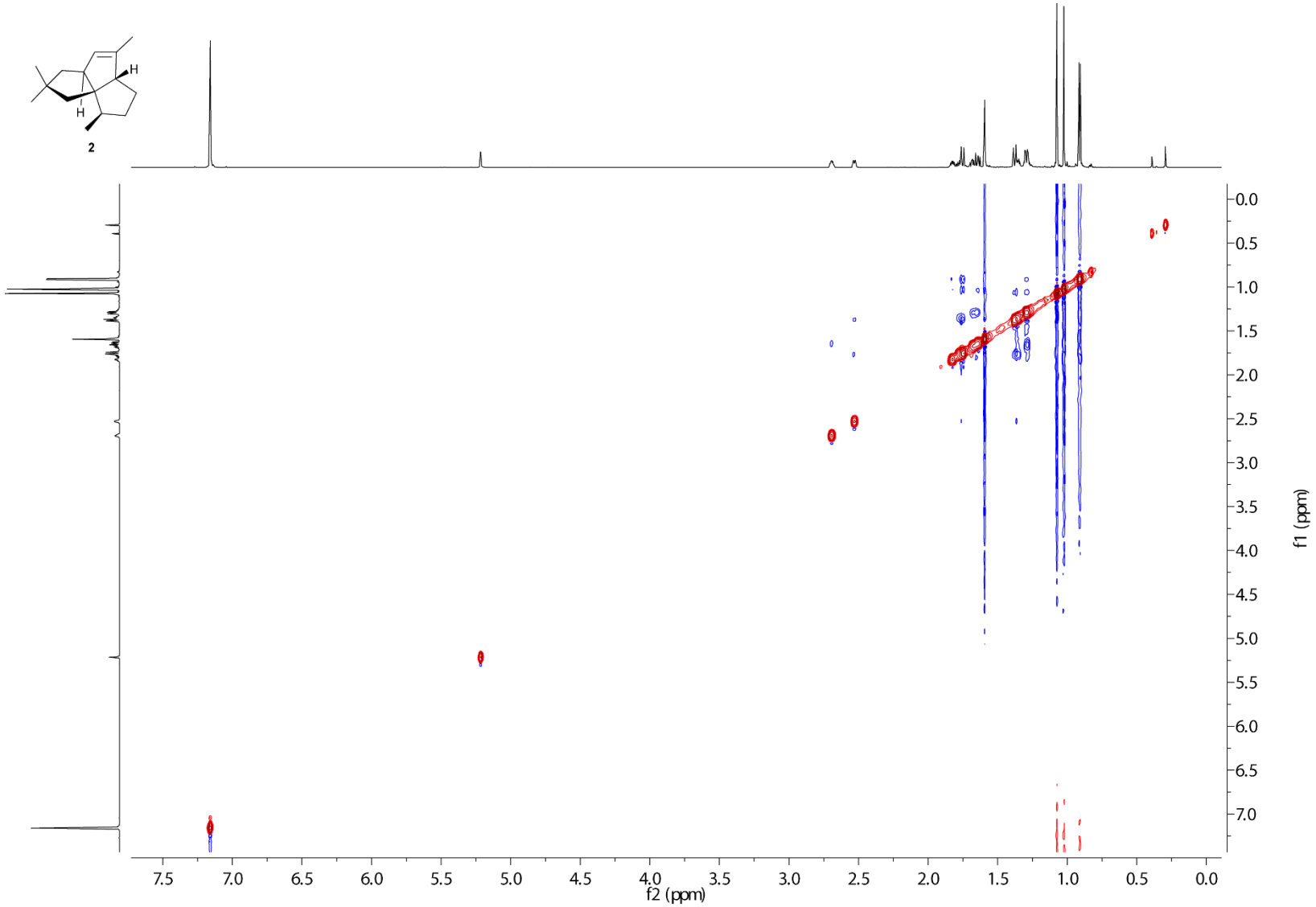

Figure S20. NOESY spectrum of **2** (C_6D_6).

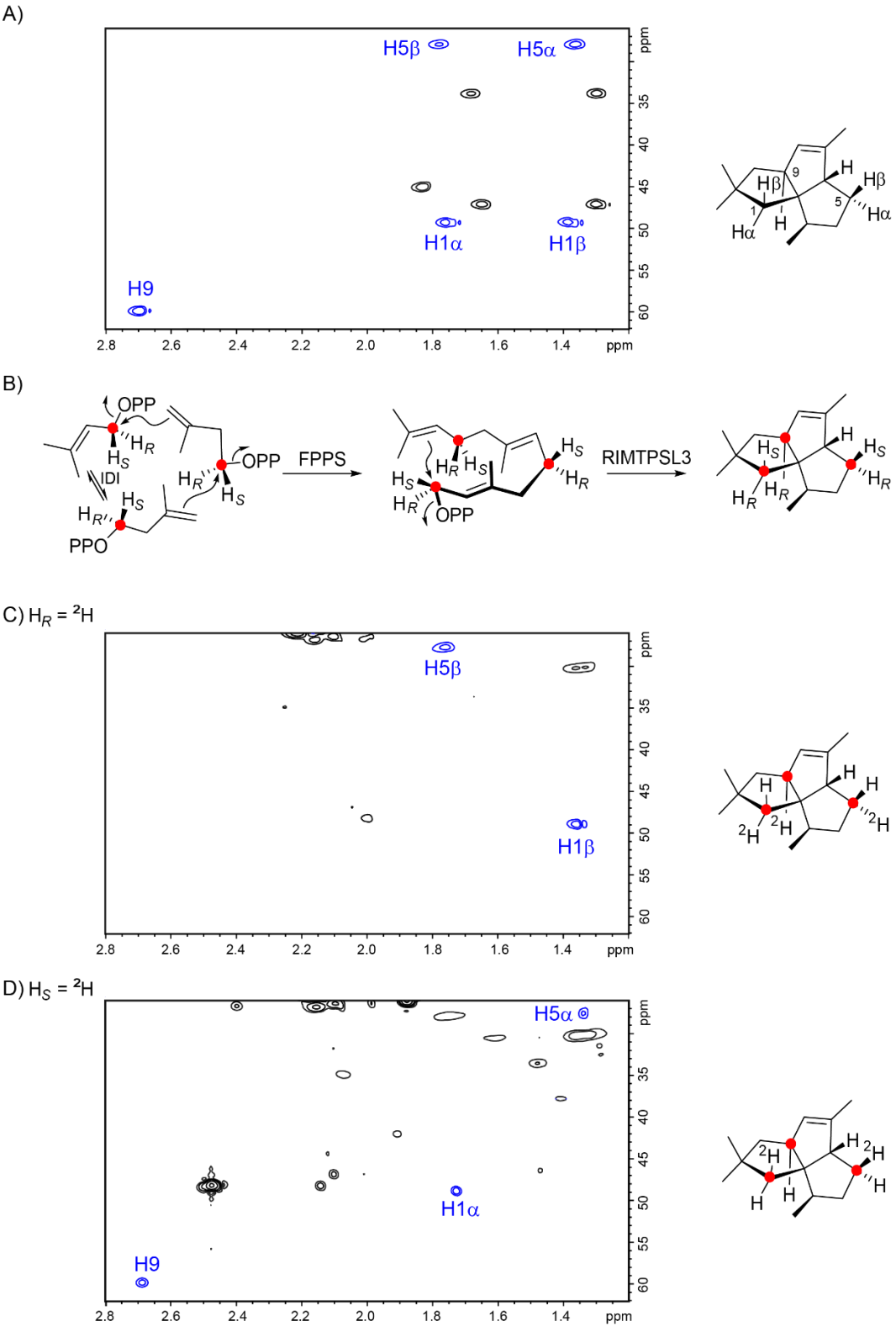

Figure S21. The absolute configuration of minor product **2**. A) Partial HSQC spectrum of unlabelled **2** showing the signals for the diastereotopic hydrogens connected to C1 and C5 and the signal for H9. B) Formation of labelled **2** from (*R*)- or (*S*)-(1-^{13}C,1-^{2}H)IPP with IDI, FPPS and RIMTPSL3. HSQC spectra for C1 and C5 of labelled **2** obtained from C) (*R*)-(1-^{13}C,1-^{2}H)IPP and D) (*S*)-(1-^{13}C,1-^{2}H)IPP. The artificially introduced stereogenic anchors allow to conclude on the absolute configuration of **2** by solving the relative configuration of the naturally present stereogenic centers with respect to these anchors. In addition, D) shows a signal for H9 that is not observed in C). In conclusion, H_R is retained at C9.

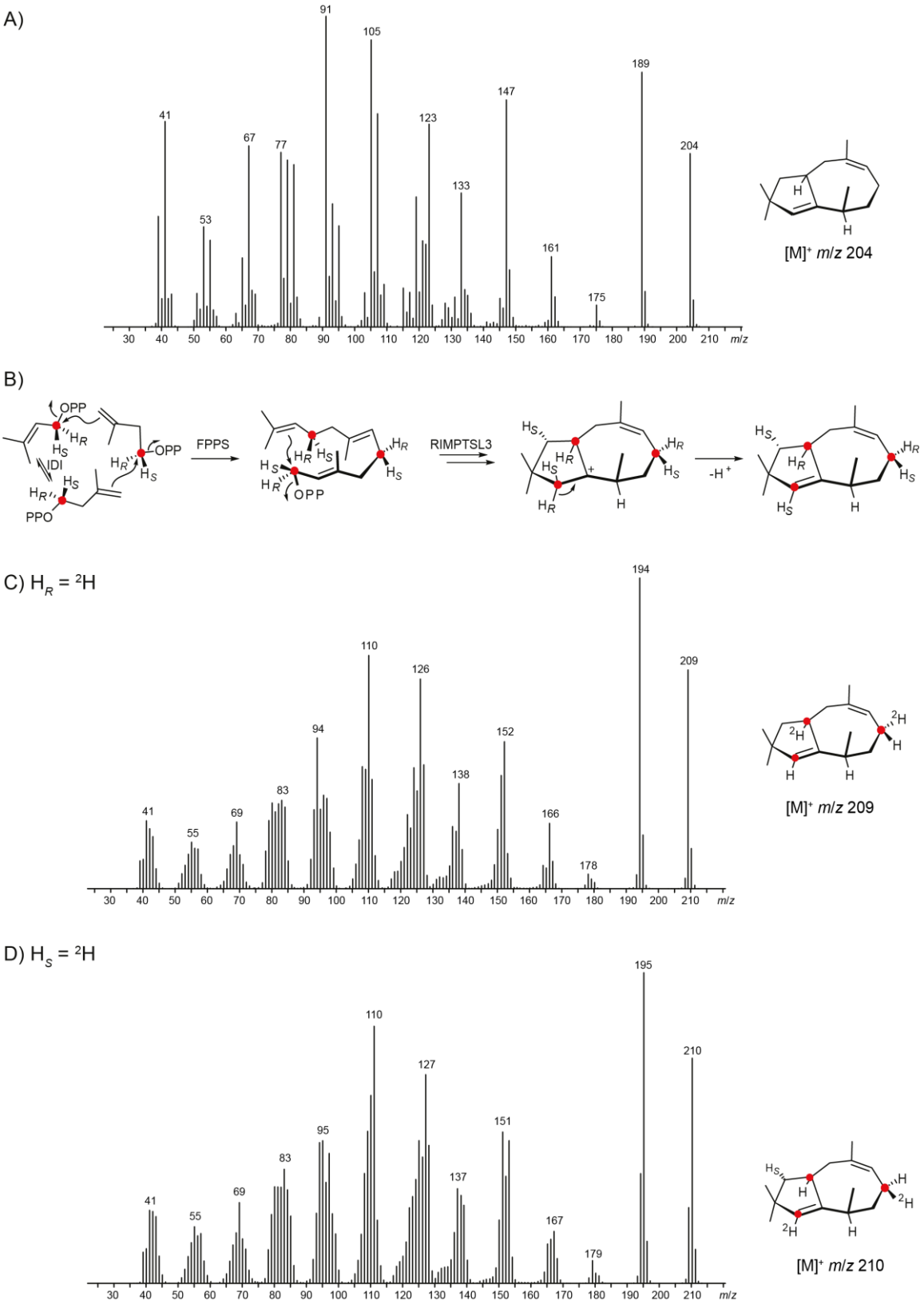

Figure S22. The final deprotonation to **1**. A) EI mass spectrum of unlabelled **1**, B) biosynthesis of labelled **1** from (*R*)- and (*S*)-(1-^{13}C,1-^{2}H)IPP, C) EI mass spectrum of labelled **1** obtained from (*R*)-(1-^{13}C,1-^{2}H)IPP, and D) EI mass spectrum of labelled **1** obtained from (*S*)-(1-^{13}C,1-^{2}H)IPP. The molecular ion at *m*/*z* 210 in D) shows retainment of deuterium, while the molecular ion at *m*/*z* 209 in C) indicates loss of deuterium.

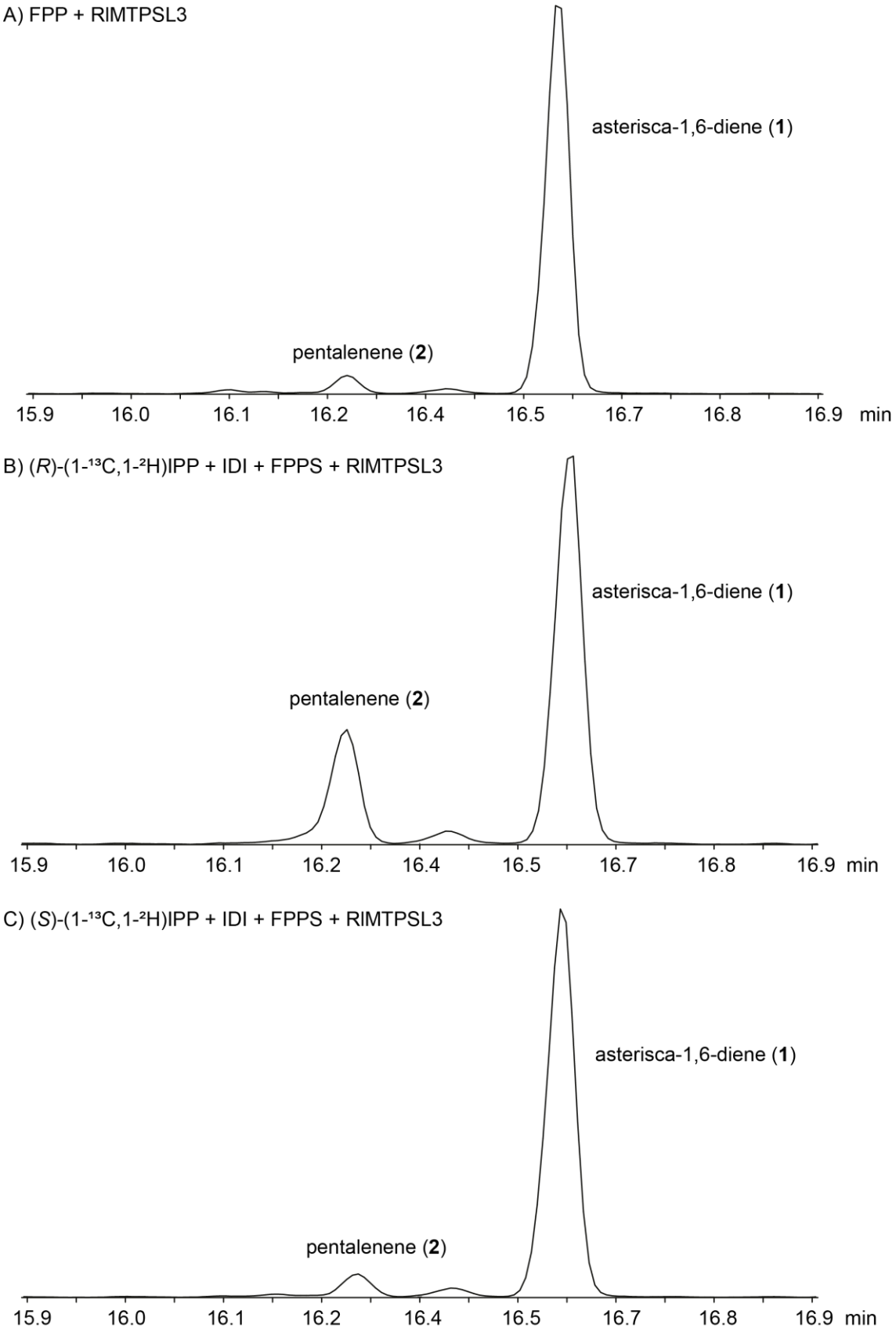

Figure S23. GC analyses of asterisca-1,6-diene (**1**) and pentalenene (**2**) produced by the enzymatic conversions of A) FPP with RIMTPSL3, B) (*R*)-(1-^{13}C,1-^{2}H)IPP with IDI, FPPS and RIMTPSL3, and C) (*S*)-(1-^{13}C,1-^{2}H)IPP with IDI, FPPS and RIMTPSL3. The production of **2** in the experiment with (*R*)-(1-^{13}C,1-^{2}H)IPP is strongly enhanced.

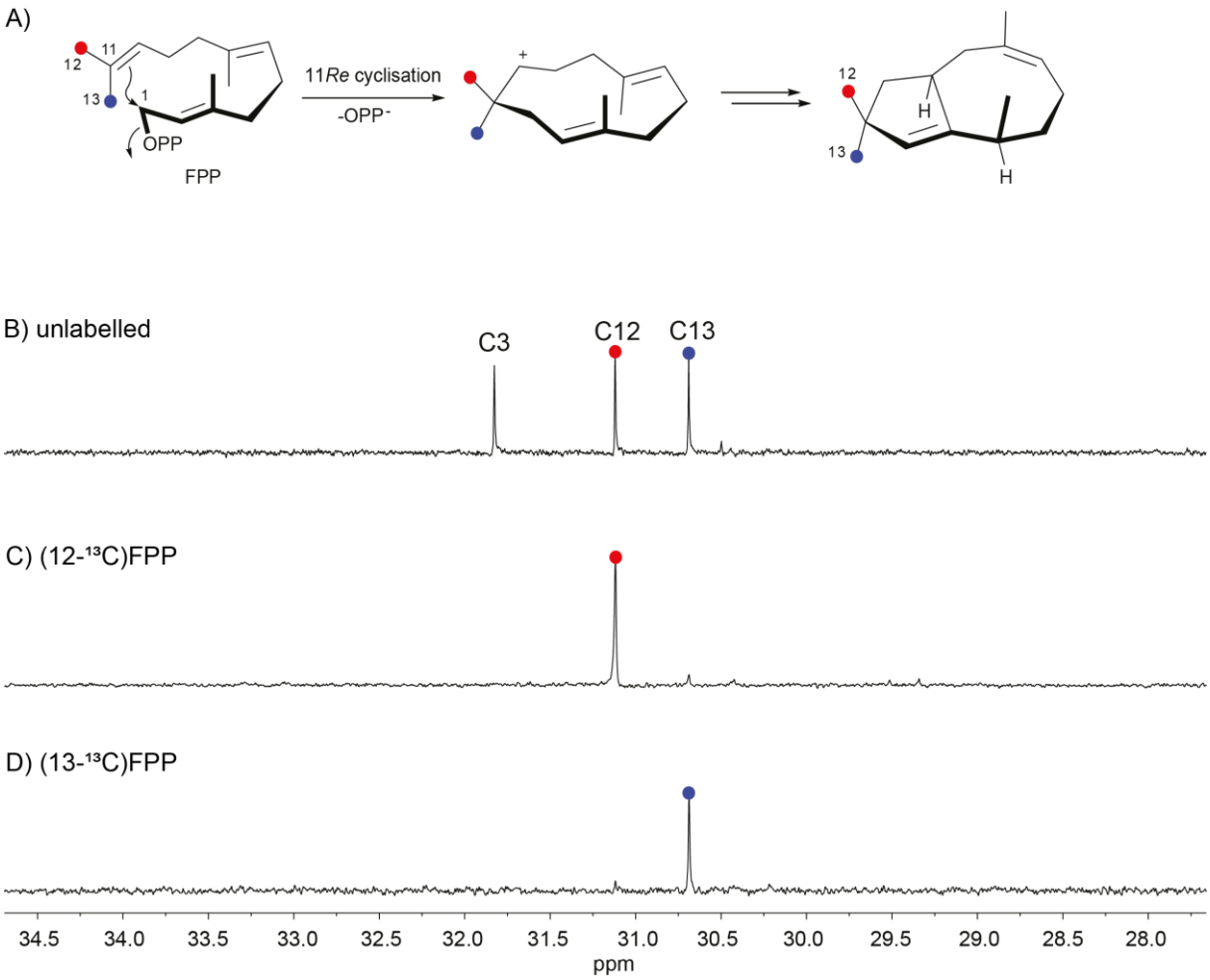

Figure S24. Investigation of the stereochemical course of the initial 1,11-cyclisation in the reaction cascade to **1**. A) Biosynthesis of labelled **1** from (12-^{13}C)FPP and (13-^{13}C)FPP (prepared with FPPS from (9-^{13}C)GPP and IPP), B) ^{13}C NMR spectrum of unlabelled **1** showing the region for C12 and C13, ^{13}C NMR spectra of the extracts obtained from enzymatic reactions with C) (12-^{13}C)FPP and D) (13-^{13}C)FPP using RIMTPSL3. The minor peaks for C13 in C) and for C12 in D) are explained by minor contaminations of the synthetic substrate (12-^{13}C)FPP with (13-^{13}C)FPP and of (13-^{13}C)FPP with (12-^{13}C)FPP.

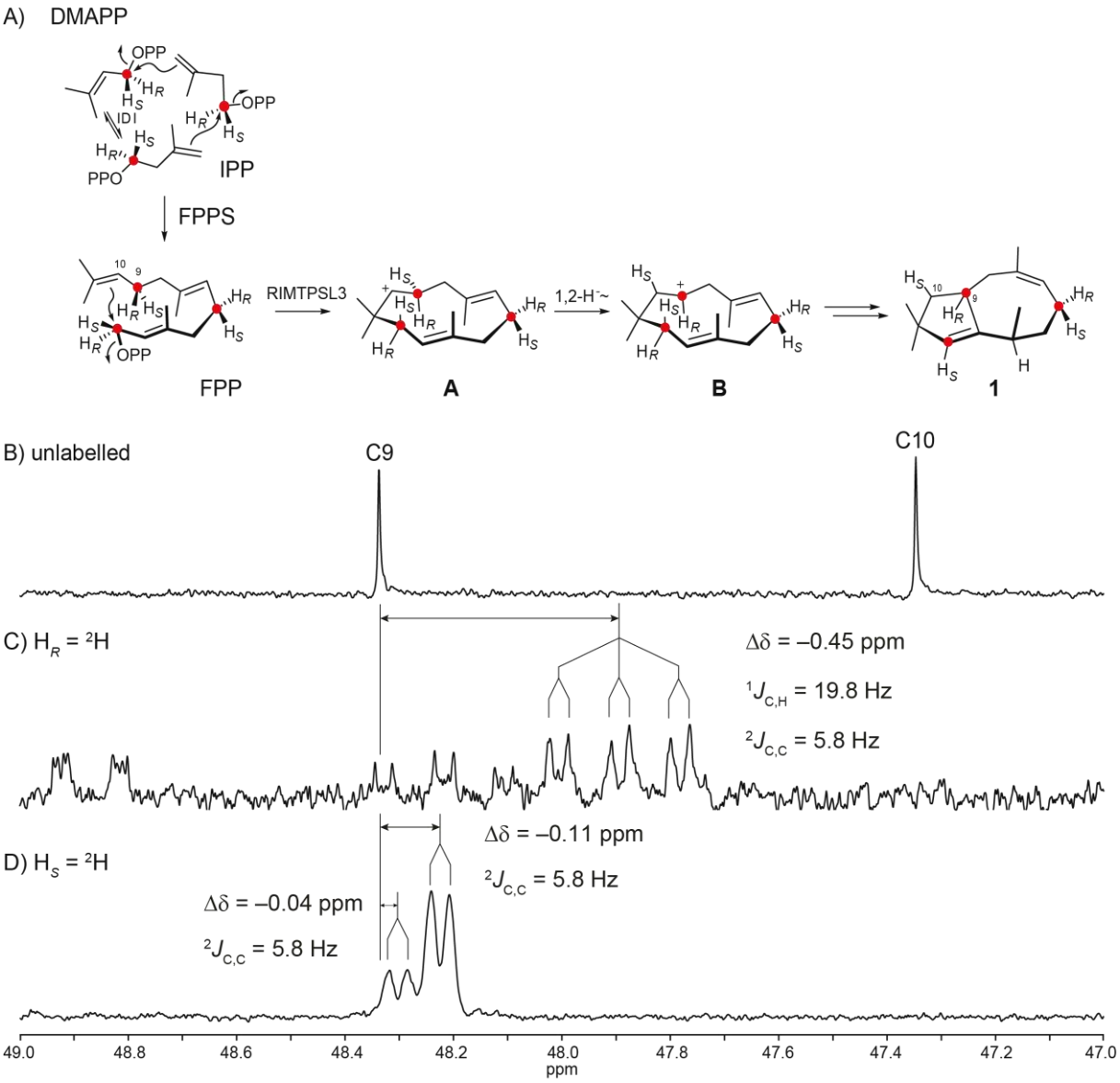

Figure S25. The 1,2-hydride shift from **A** to **B**. A) Cyclisation mechanism for labelled **1** using (*R*)- and (*S*)-(1-^{2}H, 1-^{13}C)IPP. B) Partial ^{13}C-NMR spectrum of unlabelled **1** showing the region for C9. C) ^{13}C-NMR spectrum for C9 of the obtained labelled product from (*R*)-(1-^{2}H, 1-^{13}C)IPP. D) ^{13}C-NMR spectrum for C9 of the obtained labelled product from (*S*)-(1-^{2}H, 1-^{13}C)IPP. The large doublet in D) results from the $^{2}J_{C,C}$ coupling of C9 with C1, and the upfield shift of –0.11 ppm results from deuterium atoms residing at the neighbouring carbons C1 and C10. The small doublet in D) results from the $^{2}J_{C,C}$ coupling of C9 with C1, and the upfield shift of –0.04 ppm results from a deuterium atom residing at the neighbouring carbon C1, while deuterium is lost from C10.

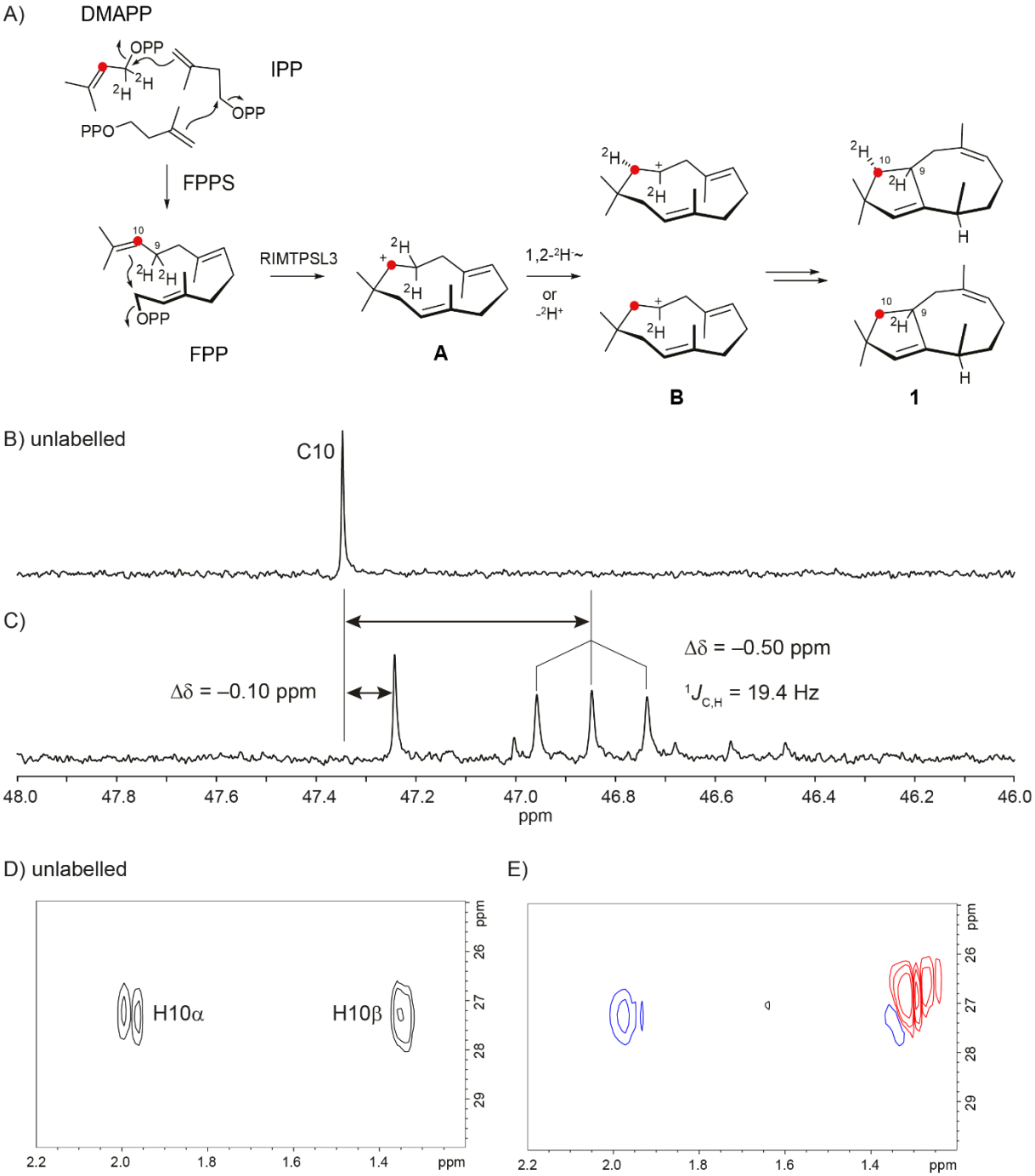

Figure S26. The 1,2-hydride shift from **A** to **B**. A) Cyclisation mechanism for labelled **1** prepared from (1,1-^{2}H,2-^{13}C)DMAPP and IPP. B) Partial ^{13}C-NMR spectrum of unlabelled **1** showing the region for C10. C) ^{13}C-NMR spectrum for C10 of the obtained labelled product. The upfield shifted triplet ($\Delta\delta$ = –0.50 ppm) for C10 in C) confirms the 1,2-hydride shift from C9 to C10. A fraction of the sample is formed with loss of deuterium, resulting in the upfield shifted singlet ($\Delta\delta$ = –0.10 ppm). This small upfield shift is a consequence of deuterium bound to C9. D) Partial HSQC spectrum of unlabelled **1** showing the region for C10. E) HSQC spectrum for C10 of the obtained labelled product. The upfield shifted crosspeak (red) for H-10β is for the compound deuterated at C9 and C10. A corresponding signal for H-10α is missing indicating that deuterium migrates into the position of H-10α. Besides the red crosspeak, two crosspeaks marked in blue are observed that represent **1** with a lost deuterium. As a consequence, the signals are less strongly upfield shifted and crosspeaks for both H-10α and H-10β are observed.

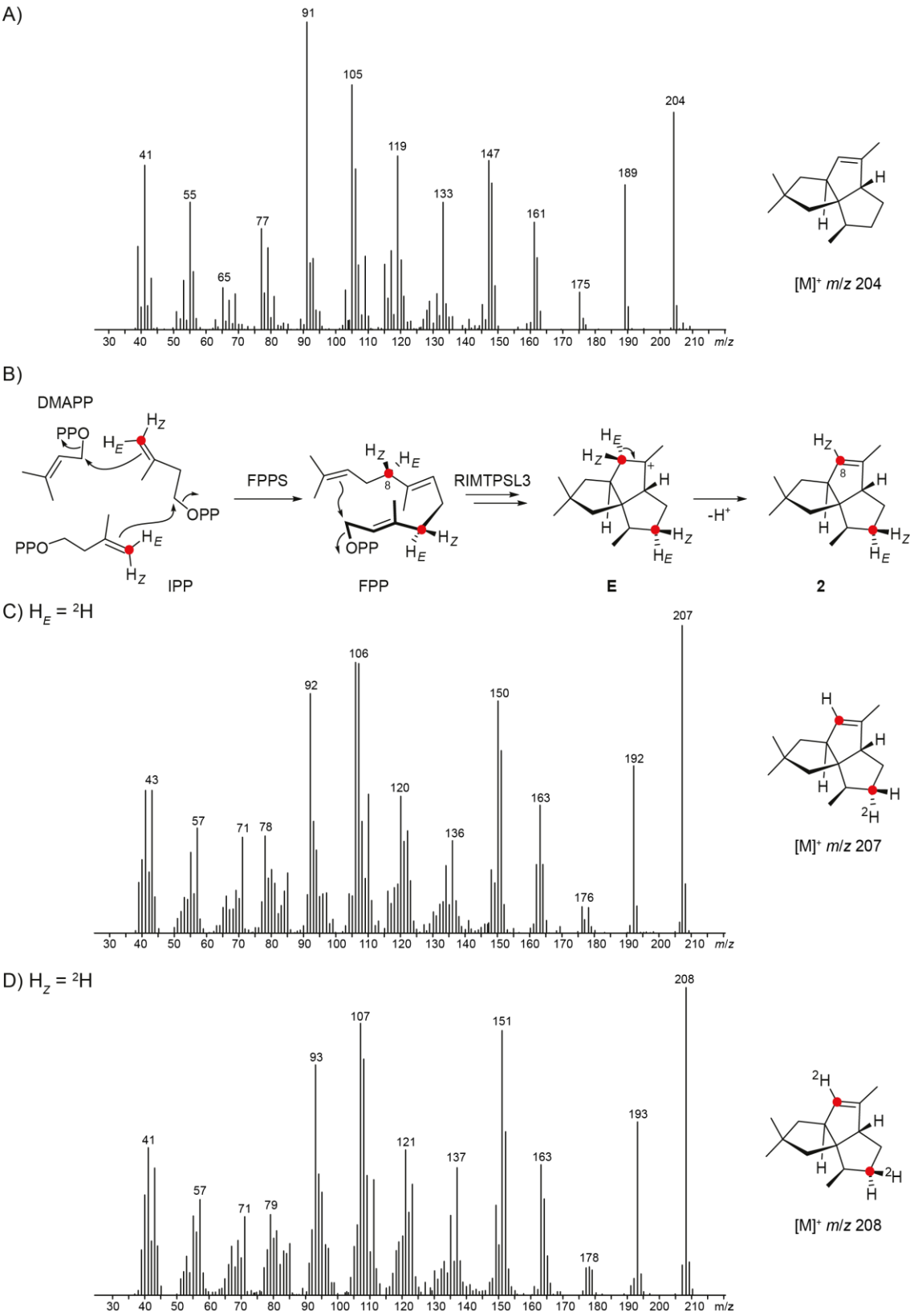

Figure S27. The final deprotonation to **2**. A) EI mass spectrum of unlabelled **2**, B) biosynthesis of labelled **2** from (*E*)- and (*Z*)-(4-^{13}C,4-^{2}H)IPP, C) EI mass spectrum of labelled **2** obtained from (*E*)-(4-^{13}C,4-^{2}H)IPP, and D) EI mass spectrum of labelled **2** obtained from (*Z*)-(4-^{13}C,4-^{2}H)IPP. The molecular ion at *m*/*z* 208 in D) shows retainment of deuterium, while the molecular ion at *m*/*z* = 207 in C) indicates loss of deuterium. Taken together, these results demonstrate the selective abstraction of H_E from C8 in the deprotonation to **2**.

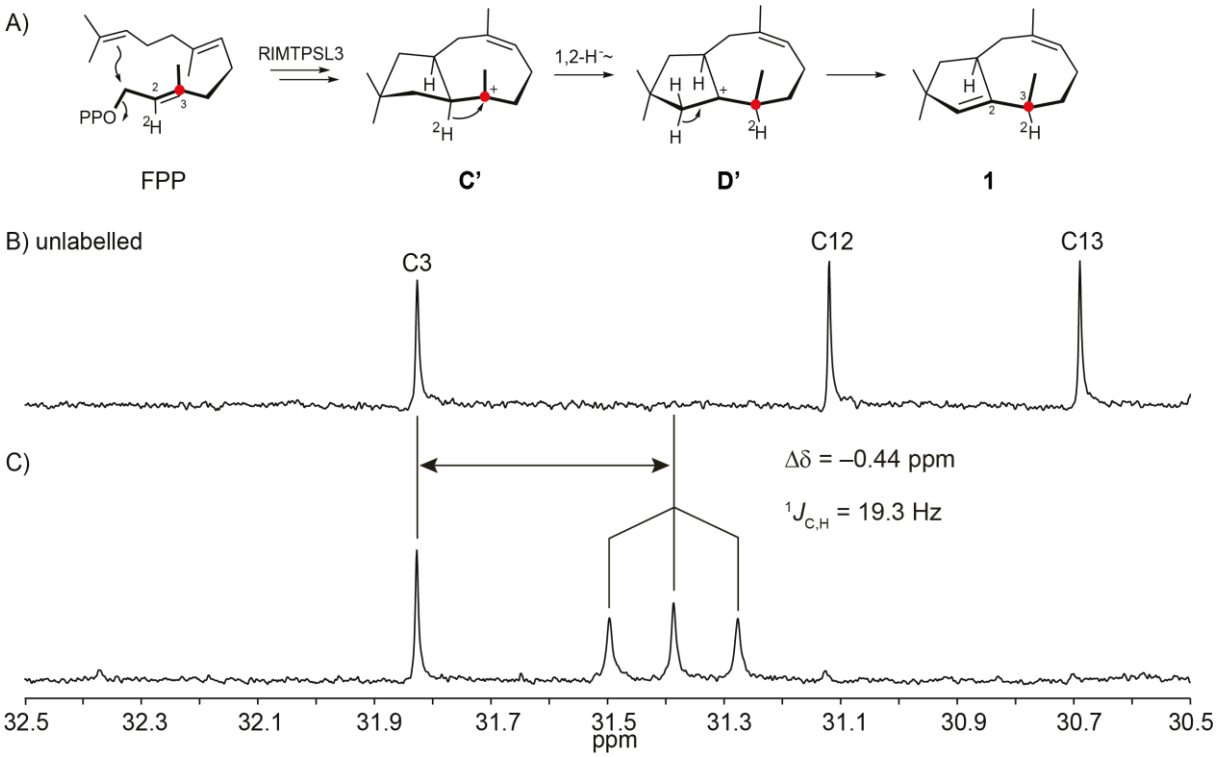

Figure S28. The 1,2-hydride shift from **C'** to **D'**. A) Enzymatic conversion of (2-^{2}H,3-^{13}C)FPP and RIMTPSL3 into labelled **1**. ^{13}C-NMR spectra of B) unlabelled **1** showing the region for C3, and C) labelled **1** obtained from (2-^{2}H,3-^{13}C)FPP. The upfield shifted triplet for C3 in C) confirms the 1,2-hydride shift from **C'** to **D'**.

References

1 G. R. Fulmer, A. J. M. Miller, N. H. Sherden, H. E. Gottlieb, A. Nudelman, B. M. Stoltz, J. E. Bercaw and K. I. Goldberg, *Organometallics*, 2010, **29**, 2176-2179.

2 H. Fan, G. Wei, X. Chen, H. Guo, B. Crandall-Stotler, T. G. Köllner and F. Chen, *Phytochemistry*, 2021, **190**, 112847.

3 C. A. Citron, J. Gleitzmann, G. Laurenzano, R. Pukall and J. S. Dickschat, *ChemBioChem*, 2012, **13**, 202-214.

4 P. Rabe, J. Rinkel, B. Nubbemeyer, T. G. Köllner, F. Chen and J. S. Dickschat, *Angew. Chem. Int. Ed.*, 2016, **55**, 15420-15423.

5 L. Lauterbach, J. Rinkel and J. S. Dickschat, *Angew. Chem. Int. Ed.*, 2018, **57**, 8280-8283.

6 P. Rabe, J. Rinkel, B. Nubbemeyer, T. G. Köllner, F. Chen and J. S. Dickschat, *Angew. Chem. Int. Ed.*, 2016, **55**, 15420-15423.

7 J. Rinkel and J. S. Dickschat, *Org. Lett.*, 2019, **21**, 2426-2429.

8 P. Rabe L. Barra, J. Rinkel, R. Riclea, C. A. Citron, T. A. Klapschinski, A. Janusko and J. S. Dickschat, *Angew. Chem. Int. Ed.*, 2015, **54**, 13448-13451.

9 G. Bian, J. Rinkel, Z. Wang, L. Lauterbach, A. Hou, Y. Yuan, Z. Deng, T. Liu and J. S. Dickschat, *Angew. Chem. Int. Ed.*, 2018, **57**, 15887-15890.

10 T. A. Klapschinski, P. Rabe and J .S. Dickschat, *Angew. Chem. Int. Ed.*, 2016, **55**, 10141-10144.